Journal of Magnetic Resonance Open 10–11 (2022) 100052

Contents lists available at ScienceDirect

Journal of Magnetic Resonance Open

journal homepage: www.sciencedirect.com/journal/journal-of-magnetic-resonance-open

Research Article

Interfacing Liquid State Hyperpolarization Methods with NMR Instrumentation

Pierce Pham, Ratnamala Mandal, Chang Qi, Christian Hilty *

Department of Chemistry, Texas A&M University, 3255 TAMU, College Station, TX 77843, USA

ARTICLE INFO

Keywords:
Hyperpolarization
Dissolution dynamic nuclear polarization
Para-hydrogen inducedPolarization

ABSTRACT

Advances in liquid state hyperpolarization methods have enabled new applications of high-resolution NMR spectroscopy. Utilizing strong signal enhancements from hyperpolarization allows performing NMR spectroscopy at low concentration, or with high time resolution. Making use of the high, but rapidly decaying hyperpolarization in the liquid state requires new techniques to interface hyperpolarization equipment with liquid state NMR spectrometers. This article highlights rapid injection, high resolution NMR spectroscopy with hyperpolarization produced by the techniques of dissolution dynamic nuclear polarization (D-DNP) and para-hydrogen induced polarization (PHIP). These are popular, albeit not the only methods to produce high polarization levels for liquid samples. Gas and liquid driven sample injection techniques are compatible with both of these hyperpolarization methods. The rapid sample injection techniques are combined with adapted NMR experiments working in a single, or small number of scans. They expand the application of liquid state hyperpolarization to spins with comparably short relaxation times, provide enhanced control over sample conditions, and allow for mixing experiments to study reactions in real time.

1. Introduction

Liquid state NMR instruments are widely available for research in chemistry and the life sciences. They support applications from routine structure determination of small molecules, to investigations of macromolecules that provide unprecedented views of molecular dynamics and its relationship to biological function [1]. The capabilities of the corresponding NMR methods are evolving on several fronts. Most visibly, higher-field magnets provide an increase both in the signal-to-noise ratio and the spectral resolution that is achievable. Barring cases with a strong magnetic field dependence of the spectral line width, the number of signals that can be resolved in a one-dimensional spectrum is approximately proportional to the NMR frequency. The achievable signal-to-noise ratio based on field strength considerations alone increases by a factor of three comparing an 11.7 T (500 MHz) magnet from the 1980's to an ultra-high field 23.4 T magnet for 1 GHz NMR available in the 2010's [2]. Designs of NMR detection probes offer versatility in the combinations of accessible nuclei and sample size. Cryoprobes provide additional sensitivity improvements though cooling of the receiver circuits. Liquid state NMR instruments are outfitted with application specific accessories, such as automation for high-throughput spectroscopy, inserts for flow NMR, imaging capabilities, and others. Spectrometer electronics presently contain digital pulse and frequency generators, which facilitate the application of NMR experiments that include techniques such as coherence selection, frequency selective excitations, frequency swept pulses, and spatially selective encoding and readout through pulsed field gradients. With these capabilities, the NMR field has seen an explosive expansion of the number of experiments and pulse sequences that have been developed in research groups around the world. These experiments are used to answer numerous questions related to molecular structure and dynamics. Modern NMR pulse sequences contain dozens of pulses, grouped into elements with different functions, for precisely controlling and reading out nuclear spin coherences.

Irrespective of the large amount of information that can be obtained, liquid state NMR does not favorably compete with other spectroscopies in the arena of sensitivity. For example, optical signals from fluorescence emissions can be measured from single molecules. Inductively detected NMR in a single scan requires on the order of nanomoles, *i.e.* 10^{14} copies of the same molecule [3]. In typical applications, even substantially larger amounts are needed. For many biological molecules, physiological concentrations are lower than what is practically detectable by NMR

* Corresponding author.
E-mail address: chilty@tamu.edu (C. Hilty).

https://doi.org/10.1016/j.jmro.2022.100052
Received 31 December 2021; Received in revised form 6 March 2022; Accepted 9 March 2022
Available online 10 March 2022

experiments. Clearly, applications of NMR could be broadened with an increase in sensitivity. In recent years, advances in hyperpolarization technologies that typically enhance sensitivity by two to four orders of magnitude have pointed in this direction. For liquid state NMR, two methods that have gained a high level of popularity are dissolution dynamic nuclear polarization (D-DNP) [4,5] and para-hydrogen induced polarization (PHIP) [6]. A variation of the latter is the method of signal amplification by reversible exchange (SABRE) [7]. These above described techniques are the primary focus for this article. Other highly capable methods exist, such as the use of dissolved noble gases [8], chemically induced dynamic nuclear polarization (CIDNP) [9], Overhauser dynamic nuclear polarization (ODNP) [117] and brute force polarization [10].

D-DNP and PHIP/SABRE enable similar usage scenarios, presenting opportunities for the study of molecules, molecular interactions and reactions in chemistry and biology by high-resolution NMR. D-DNP has been used to investigate time-resolved biological processes such as metabolism [11,12], enzyme catalysis [13,14], protein and nucleic acid folding [15–17], protein hydration [18]. It has been applied for the highly sensitive measurement of compounds pertaining to metabolomics [19,20], cellular properties [21], and for characterizing protein-ligand interactions [22–26]. It has also shown utility for the kinetic and mechanistic characterization of chemical reactions [27–30]. The PHIP technique presents unique opportunities for the characterization of organometallic complexes [31]. SABRE, the non-hydrogenative method of PHIP provides a different avenue for hyperpolarizing several types of small molecules that exhibit a binding site to a polarization transfer catalyst, such as drug compounds, on nuclei including ^{1}H [32–34], ^{15}N [35–37] and others. SABRE polarization can also be used for monitoring of chemical reactions [38], and is principally amenable to many of the other above mentioned topics as well.

While various applications in different fields have been described, these techniques are at present primarily used by research groups specializing in hyperpolarized NMR. Their still limited adoption may be partially due to the fact that corresponding instrumentation is currently unavailable in typical facilities. Nevertheless, some user facilities now offer D-DNP. Para-hydrogen on the other hand can be produced inexpensively, with a total set-up cost for hardware that is less than the typical cost of producing one or two biomolecular NMR samples. The use of para-hydrogen is compatible with shared NMR instrumentation such as that available in typical institutional facilities. Para-hydrogen based methods using the many polarization transfer catalysts that have been developed in recent years, are applicable to a broadened range of problems. The goal of this article is to describe options for interfacing these hyperpolarization methods with liquid state NMR.

2. NMR sensitivity and hyperpolarization

The basis for the utility of hyperpolarization methods lies in the population distribution of nuclear spins on the Zeeman energy levels, given by the energies of spin states in the magnetic field (Fig. 1). With the Zeeman energy difference of a spin-1/2 nucleus such as ^{1}H, ^{13}C, ^{15}N or ^{19}F, $\Delta E = \gamma\hbar B$ and the Boltzmann distribution, $n_2/n_1 = exp(-\Delta E/kT)$, it can immediately be found that

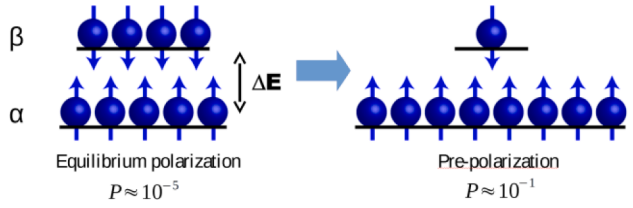

Fig. 1. Schematic representation of Zeeman energy levels and populations for the spin-up (α) and spin-down (β) states of a spin-1/2. Left: Thermal equilibrium polarization. Right: Hyperpolarization.

$$P = \frac{n_1 - n_2}{n_1 + n_2} = \frac{1 - \exp(-\Delta E/kt)}{1 + \exp(-\Delta E/kT)} = \tanh\frac{\Delta E}{2kT} \quad (1)$$

Here, γ is the gyromagnetic ratio ($\gamma_{1H} = 267.522$; $\gamma_{13C} = 67.2828$; $\gamma_{15N} = -27.116$; $\gamma_{19F} = 251.815\bullet10^{6}$ rad s^{-1} T^{-1}), $\hbar = 1.054571\bullet10^{-34}$ J s the reduced Planck constant, B the magnetic field, $k = 1.380649\bullet10^{-23}$ J K^{-1} the Boltzmann constant, and n_1 and n_2 the number of spins on the lower and the upper Zeeman energy levels, respectively.

P is the fractional population difference, in other words the population difference of the two energy levels divided by the total number of spins. This parameter is referred to as the spin polarization. Because of cancellation between absorptive and emissive processes, the signal that is observed in an NMR experiment is proportional to the spin polarization. Under thermal equilibrium at room temperature (298 K), Equation 1 indicates that $P = 4.0\bullet10^{-5}$ for ^{1}H and $P = 1.0\bullet10^{-5}$ for ^{13}C in a 500 MHz (11.7 T) NMR magnet. In other words, only a net of a few in every 100,000 spins contribute the observed signal. By way of comparison, the involved energy differences are much larger in typical optical transitions. In thermal equilibrium for optical transitions, only the ground state is appreciably populated and the absorption or emission signal is not attenuated by the opposite process.

Hyperpolarization methods prepare the nuclear spin system in a state with an enhanced population difference. A state with $P = 1$, where only the lower energy level is populated, would result in a signal enhancement of 5 orders of magnitude in liquid state NMR, in comparison to polarization at high field and room temperature. In practice, signal enhancements of 2 to 4 orders are readily achieved with different hyperpolarization methods.

The production of the hyperpolarized spin state requires a physical method other than equilibration of the spins in the magnetic field used for measurement. Excellent reviews describing different hyperpolarization methods are available [39,40]. The two methods of DNP and PHIP are briefly outlined in the following. The hyperpolarized spin state is a non-equilibrium state, which therefore relaxes to the thermal equilibrium polarization with the characteristic spin-lattice (T_1) relaxation time constant. The hyperpolarized sample must be prepared for measurement before relaxation has occurred.

2.1. Dissolution dynamic nuclear polarization

D-DNP is capable of producing liquid state spin polarization on the order of percent to tens of percent for nuclear spins that exhibit a sufficiently long spin-lattice relaxation [4]. Hyperpolarization is created in the frozen solid, where the Boltzmann distribution favors the lower energy level, after which the sample is brought to room temperature in a rapid dissolution process [41]. The generation of a near-unity nuclear spin polarization by equilibration high-field magnet alone requires a temperature in the milli Kelvin range (shown in Fig. 2a for ^{1}H or ^{13}C nuclei at a field of 11.7 T), as well as a long equilibration time due to spin-lattice relaxation time constants that can exceed days. The DNP process facilitates the generation of hyperpolarization through unpaired electron spins, which can reach a near unity polarization in the 1-Kelvin range (Fig. 2a, solid curve). Two example structures of free radicals used as polarizing agents are shown in Fig. 2b. The trityl radical OX63 is commonly employed for DNP of ^{13}C and other nuclei in aqueous solutions [42,43]. The TEMPOL nitroxide radical is efficient for hyperpolarizing nuclei such as ^{1}H and ^{19}F [44,45]. DNP in frozen solids in general is described by different mechanisms that involve flipping interacting nuclear spins and electron spins through microwave radiation [46,47]. The microwaves are irradiated near the frequency of the electron spin transition. The action of microwaves in combination with electron spin relaxation re-populates energy levels to enhance the population difference of nuclear spin energy levels. This process can be seen as using the higher polarization of electron spins to create nuclear spin

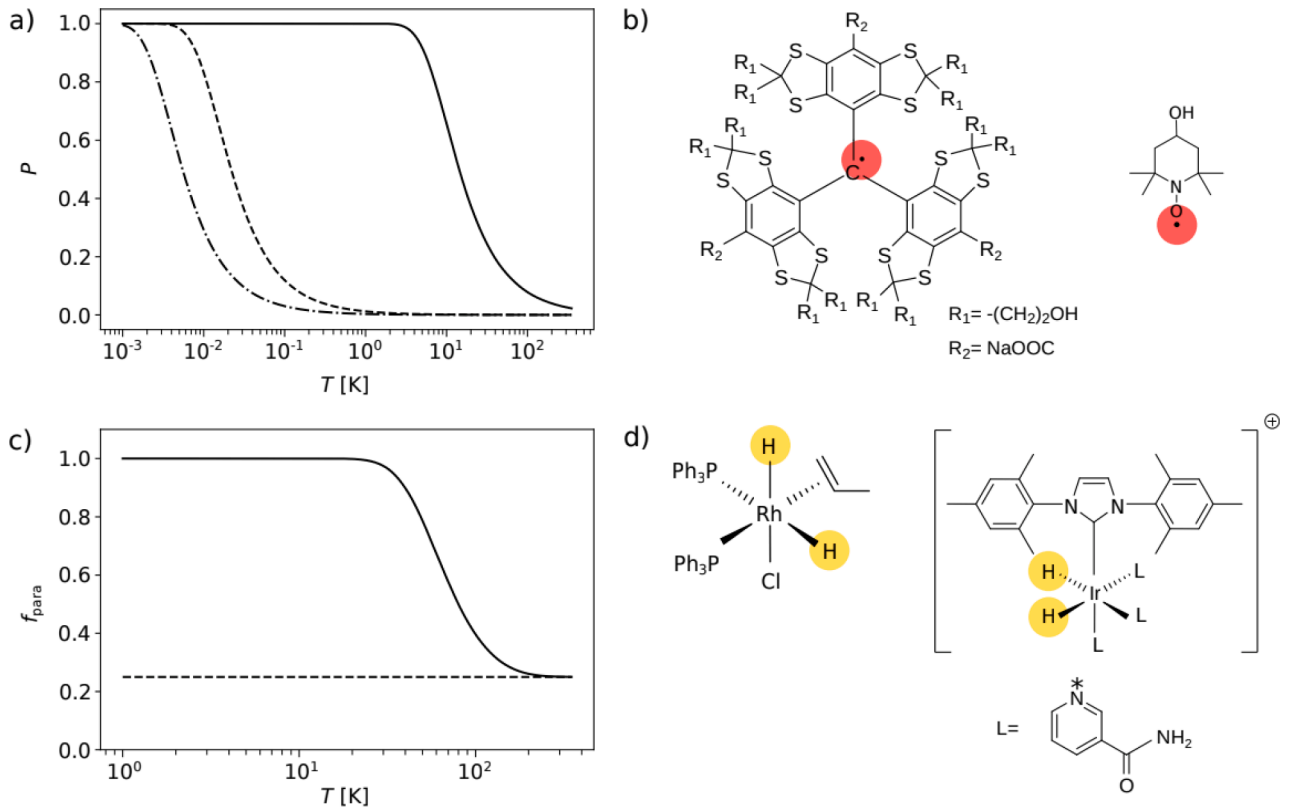

Fig. 2. a) Temperature dependence of equilibrium spin polarization in a field of 11.7 T. Spins are ^{13}C (- . -), ^{1}H (- -), and electron (–). b) Free radicals used as polarizing agents for D-DNP. tris[8-carboxy-2,2,6,6-tetrakis(2-hydroxyethyl)benzo[1,2-d:4,5-d′]bis[1,3]-dithiol-4-yl]methyl free radical (OX63; left) for ^{13}C DNP in aqueous samples. 4-hydroxy-2,2,6,6-tetramethylpiperidin-1-oxyl (TEMPOL; right) for ^{1}H and ^{19}F hyperpolarization in aqueous solution. c) Temperature dependence of equilibrium para-hydrogen fraction (–). The horizontal line is the asymptote for high temperature (- -). d) Catalysts for producing hyperpolarization derived from para-hydrogen. Wilkinson's catalyst (shown as metal hydride with bound propene; left) for the hydrogenative PHIP. (1,3-bis(2,4,6-trimethylphenyl)imidazol-2-ylidene)IrH_2L_3 with three bound substrates L = nicotinamide; right) for SABRE polarization. * indicates the binding site of L to the iridium.

polarization.

In practice, DNP requires electron spins that are unpaired and thus can be addressed using microwaves, as in electron paramagnetic resonance spectroscopy. For D-DNP, electron spins are mostly added to the sample as organic free radicals. The DNP mechanism is general in the sense that different nuclei can be hyperpolarized by a change in the microwave frequency. An important advantage of D-DNP is the ability to work with many different types of molecules. The primary limitation is, firstly, the solubility and the requirement that the molecule of interest and free radical are dispersed when frozen. The aliquot that is made for hyperpolarization can be a small volume, such as a microliter, and it becomes diluted upon dissolution. Secondly, the spin-lattice (T_1) relaxation of the sample should be sufficiently long for preserving the spin polarization during the dissolution process. Due to this consideration, D-DNP is primarily applied with spin-1/2 nuclei that are not subject to quadrupolar relaxation, with the exception of nuclei with long T_1 relaxation times such as ^{2}H, ^{6}Li [48] or ^{7}Li [49]. Small molecules are most readily hyperpolarized because of reduced spin relaxation, although macromolecules such as unfolded proteins have also been directly hyperpolarized [15,50].

2.2. Para-hydrogen induced polarization

The wave function of hydrogen molecules is composed of the electronic, vibrational, rotational, translational, nuclear, and spin wave functions and follows the symmetry condition arising from the Pauli Principle. Para-hydrogen molecules have symmetric rotational wave functions with even rotational quantum number J, and consequently antisymmetric nuclear spin wave functions with total spin $I = 0$. The nuclear spin state of para-hydrogen is a singlet state. In contrast, the orthohydrogen with odd J contains a nuclear triplet spin state with $I = 1$ [51]. The relative populations of the para and ortho states of hydrogen are dictated by Boltzmann's distribution of the rotational energy levels,

$$\frac{N_{para}}{N_{ortho}} = \frac{\sum_{even\ J}(2J+1)\exp\left(\frac{-J(J+1)\theta_R}{T}\right)}{3\sum_{odd\ J}(2J+1)\exp\left(\frac{-J(J+1)\theta_R}{T}\right)} \quad (2)$$

The rotational temperature $\theta_R = 87.6$ K depends on the moment of inertia of the hydrogen molecule Equation 2. can be used as a basis to calculate the fraction of para-hydrogen (Fig. 2b). The para-hydrogen fraction reaches ~99.9% at its boiling point of 20.3 K and ~50% at liquid nitrogen temperature of 77 K.

In a hydrogenation reaction using a molecular catalyst, the singlet state of a para-hydrogen molecules is conserved in the hydrogenated products. A classical example of a hydrogenation catalyst to produce nuclear spin hyperpolarization is Wilkinson's catalyst [52]. One of its active species shown in Fig. 2d has an octahedral geometry, with metal hydrides cis to a bound olefin substrate. This structure allows the hydride insertion at the olefin double bond. At a high magnetic field in the Tesla range, the singlet state of parahydrogen is distributed equivalently to two singlet states in the hydrogenated product by the Parahydrogen And Synthesis Allow Dramatically Enhanced Nuclear Alignment (PASADENA) process. If hydrogenation initially occurs at low field, Adiabatic Longitudinal Transport After Dissociation Engenders Nuclear Alignment (ALTADENA) produces only one αβ state with the lower energy in the hydrogenated product. A non-hydrogenative method, named Signal Amplification By Reversible Exchange (SABRE) [7],

hyperpolarizes multiple classes of organic molecules such as nitrogen heterocycles, amines, and O-donors that bind reversibly to a polarization transfer catalyst (Fig. 2d) [53]. The principle of SABRE can be explained by the level anti-crossing (LAC) theory. In a spin system including the two hydride and a ligand spin, a singlet-to-triplet conversion of the hydride can occur simultaneously with polarization of the ligand spin. When the coupling between the hydride ($J_{HH'}$) dominates, LAC occurs when the difference of the frequency of the two hydride spins and the ligand spins is $\nu_H - \nu_X = J_{HH'}$ [54]. With typical constants, LAC of ^{1}H SABRE occurs in the millitesla range, while other nuclei such as ^{15}N and ^{13}C are polarized at magnetic fields below 1 μT.

The implementations of all three para-hydrogen polarization mechanisms described above present several advantages. First, the generation of para-hydrogen is achieved at low cost. Any equipment required can be set up in a non-specialized research lab. Second, para-hydrogen can be transported in a non-magnetic container, such as an aluminum bottle and used over the course of several days. Therefore, para-hydrogen production does not need to occur in the same location as NMR spectroscopy. Third, the SABRE technique and to a limited extent also the hydrogenative PASADENA/ALTADENA experiments can be repeated multiple times for signal averaging or other purposes. In the case of the hydrogenative mechanisms, repetition is possible because reactions often do not complete within a single experimental time, so that additional hyperpolarized product can be produced after re-introduction of hydrogen gas. A primary challenge in the application of para-hydrogen polarization is the need for a suitable hydrogenation or polarization transfer catalyst, and compatible substrate for hyperpolarization. Presently, significant developments in the available SABRE catalysts for the

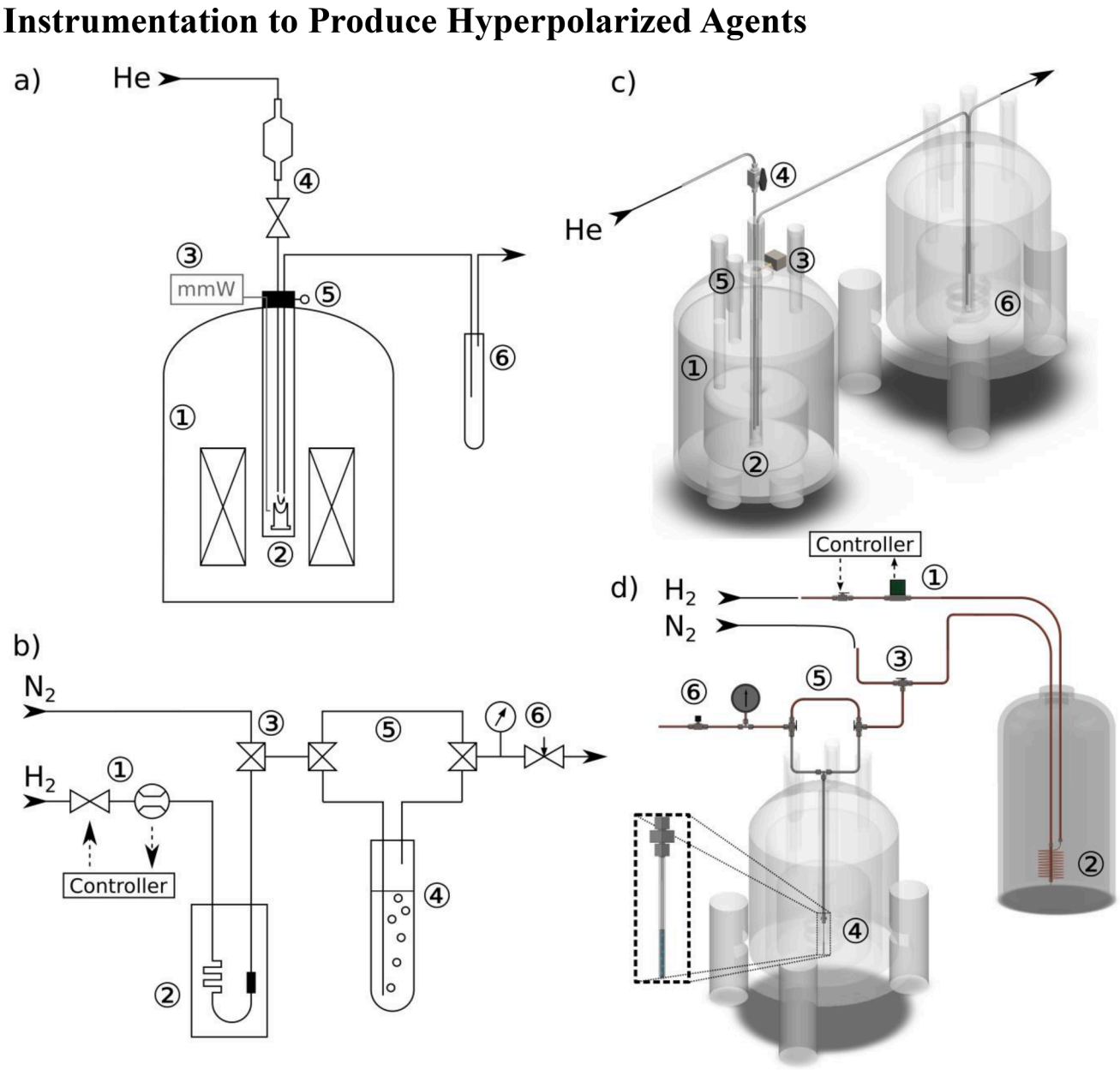

Fig. 3. Instrumentation for producing hyperpolarization. a) D-DNP polarizer. ①–Superconducting magnet with variable temperature insert. ②–Sample holder in microwave cavity. The flow path for dissolution of the solvent after hyperpolarization is indicated. ③–Millimeter wave source. ④–Heated solvent vessel with discharge valve. ⑤–Access port for sample loading and dissolution apparatus. ⑥–Sample tube. b) Para-hydrogen polarizer. ①–Hydrogen gas gate valve with flow sensor. ②–Cryogenically cooled heat exchanger and spin-flip catalyst (black). ③–Selection valve for hydrogen or purge gas. ④–Sample tube with capillary. ⑤–Bypass tubing and path selection valves. ⑥–Pressure gauge and flow control valve. c) and d) Illustration of instruments in a and b, respectively.

hyperpolarization of multiple types of substrates in different solution conditions are being made [55,56].

3. Instrumentation to produce hyperpolarized agents

Both D-DNP and para-hydrogen polarization require cryogenic cooling, in the former case populating a lower of two electron spin Zeeman energy levels, and in the latter case populating the lowest rotational energy of H_2. Requirements are less strict for the production of para-hydrogen, for which the maximum enrichment is achieved at a higher temperature around 20 K, in the absence of a high magnetic field and without the need for radio-frequency or microwave fields to saturate a spin transition. On the other hand, the para-hydrogen as a product of this procedure does not itself yield an NMR signal, but requires a reaction or molecular interaction for generating usable hyperpolarization. The following sections describe examples for instrumentation for both methods.

3.1. Dissolution DNP

D-DNP is achieved in a superconducting magnet, typically in the field range between 3.35 T and 11.7 T [5,57] (Fig. 3a). This magnet contains a variable temperature bore, which can be cooled to a temperature near 1 K. To prevent contamination of the cold surfaces of this chamber with atmospheric gases and water, a strict access control is implemented, by an access valve at the top of the magnet. The superconducting magnet itself, as well as the sample chamber, are cooled by liquid helium or in some implementations by a closed cycle cryocooler [58]. D-DNP systems that cool the sample using liquid helium require a vacuum to reach a temperature below 4.2 K at atmospheric pressure, for example to reach a temperature of 1.4 K at a vapor pressure of 2.8 mbar. This cooling consumes helium through boiling. Microwaves are delivered through a waveguide from a source on the outside of the magnet, to the sample with in the cold bore. The sample is typically located in a non-resonant microwave cavity connected to the waveguide. The frequency of the microwave source is adjusted to the magnetic field, $f = gB\mu_B/h$, with $g \approx 2.0023$ the electron g-factor and $\mu_B = 9.27401\ \mathrm{J\,T^{-1}}$ the Bohr magneton. The resulting frequency is in the range of 94 – 328 GHz for the magnetic fields stated above. At the temperature of $\sim$ 1 K, the electron spin relaxation time is sufficiently long to enable saturation using a microwave power of $<$ 100 mW. Microwaves with this power level can be generated using diodes. Therefore, D-DNP does not depend on high-power gyrotrons that would be needed to saturate electron spins at a higher temperature [59]. After polarization, D-DNP systems dissolve the sample in a stream of a heated solvent, and flush it out of the cold region of the instrument. After this step, the sample is ready to be used for liquid state NMR spectroscopy. The generated spin polarization is usable within 3 – 5 times of the T_1 relaxation time, which requires spectra to be acquired rapidly.

3.2. Para-hydrogen induced polarization

The production of para-hydrogen is readily implemented in a laboratory without highly specialized instrumentation. Cryogenic liquid hydrogen spontaneously converts to the para spin isomer, a process that can be accelerated by the addition of a spin-flip catalyst with magnetic properties, such as iron(III) oxide. At the boiling point of 20 K, hydrogen gas has a para spin isomer content of 99.8 % (Fig. 2b). For safety reasons, most laboratories produce para-hydrogen from a source in the gas phase, which is cooled in a heat exchanger. An example implementation, which can be constructed portably and for a negligible cost, is shown in Fig. 3b. Hydrogen gas flows into the system through a gate valve, which again for safety reason is controlled by a flow sensor. The gas then passes through a coil of copper tubing serving as a heat exchanger, which in the diagram is immersed in liquid nitrogen to reach a temperature of 77 K. After cooling, the gas flows through a section of tubing containing a few grams of granular iron(III) oxide. At this temperature, the para-hydrogen content is enriched to 52%, up from 25 % at room temperature. The gas subsequently exits the cold region. Stainless steel tubing is used as entry and exit point into the cold region to reduce heat transfer. In order to achieve a higher para spin isomer enrichment, the liquid nitrogen cooled heat exchanger can be replaced with a cryocooler that achieves a temperature of near 20 K [60]. Thereby, a three times higher deviation from the equilibrium para content is achieved. After para-hydrogen enrichment, the gas is delivered to a sample containing either a reaction mixture with a hydrogenation catalyst, or a mixture with polarization transfer catalyst for SABRE. As shown in the figure, the hydrogen gas is bubbled into the sample through a capillary. Two three-way valves with bypass tubing allow to switch the bubbling process on or off. At the outlet of the apparatus, a needle valve regulates the flow rate. The flow constriction introduced by the needle valve allows experiments at an elevated pressure of up to 10 bar or more. Likewise, the reaction mixture in the NMR tube can be left pressurized with hydrogen gas for catalyst activation prior to an experiment, as needed. The pressure is primarily limited by the NMR tube (a medium or high pressure NMR tube or other sample container is required), as well as by the flow path and the cooled container for the spin-flip catalyst. Optionally, in the system as drawn, nitrogen gas can be introduced for purging before introducing air sensitive catalysts.

In the absence of a magnetic spin-flip catalyst, the para spin-state of hydrogen can persist for days [33]. Para-hydrogen gas that has been produced can be batch filled, stored and transported in a medium-pressure gas cylinder. This option is of interest for using para-hydrogen in conjunction with facility NMR instruments where cryogenic cooling would be difficult to set up.

Safe handling of hydrogen gas requires precautions. Hydrogen gas is flammable, can spontaneously ignite after flowing through tubing and building up a static charge, and can form explosive mixtures with air. Electrically grounded metal tubing should be used with hydrogen gas. The gas should be vented to the outside of the building. If vented through building systems, it should first be diluted to well below the lower explosive limit of 4 % by volume in air.

3.3. Signal enhancements

Instead of the spin polarization, hyperpolarized liquid state NMR experiments are sometimes characterized with a signal enhancement parameter $\varepsilon = S_{\mathrm{hp}} / S_{\mathrm{thermal}}$, where S_{hp} is the signal integral with hyperpolarizaiton, and S_{thermal} a reference signal of the same sample without hyperpolarization, *i.e.* at a population distribution under thermal equilibrium. The signal enhancement of an experiment therefore depends on the magnetic field of measurement, as well as on the measurement temperature. In the case of a D-DNP experiment, this parameter can be expressed as

$$\in = \frac{P_{\mathrm{DNP}}^{\mathrm{LT}}}{P_0^{\mathrm{LT}}} \frac{P_0^{\mathrm{LT}}}{P_0^{\mathrm{HT}}} \alpha_{\mathrm{loss}} \tag{4}$$

Here, LT and HT designate low and high temperature, respectively. P_{DNP} is the polarization achieved with DNP, and P_0 the polarization under thermal equilibrium. The first fraction is capped by the ratio of electron and nuclear spin frequencies, the second fraction is approximately equal to the ratio of high and low temperatures, and the α_{loss} factor describes the polarization losses during dissolution and sample transfer. Typical signal enhancements for DNP, for example for ^{13}C, range from $>$1000 to values of 10^4 or more, in comparison to NMR signal at $\sim$10 T and room temperature. These signal enhancements correspond to nuclear spin polarizations on the level of percent to tens of percent.

Para-hydrogen based methods convert the spin order of para-hydrogen to spin polarization. The signal enhancement is in principle capped by ratio of the para-hydrogen fraction to the thermal polariza-

tion of proton. For example, the highest enhancement of PASADENA is formulated below [51]:

$$\in = \frac{kT\left(1 - 4f_{\text{para}}\right)}{6\gamma\hbar B_0} \quad (5)$$

In practice, the different para-hydrogen methods yield different signal enhancements. The hydrogenative methods of PASADENA / ALTADENA are often found to provide enhancements of >10,000, although these can be difficult to quantify because of the on-going reaction. SABRE readily provides signal enhancements of up to 1,000 or more, while requiring no modification of the molecules involved and being repeatable.

4. Interfacing liquid hyperpolarization with high-field NMR

The D-DNP and para-hydrogen polarization mechanisms ultimately both produce liquids with hyperpolarized solutes using agents that are external to the NMR magnet. These liquids are intended for a wide range of applications enhancing high-resolution NMR, including non-equilibrium reactions, molecular interactions in chemistry or biochemistry, multidimensional NMR spectroscopy for targeted structure determinations in complex molecular systems, the solvation of macromolecules, protein folding, and others. Enabling these applications requires interfacing the liquid state hyperpolarization equipment with an NMR spectrometer. This task involves similar requirements, and thus similar approaches for the described hyperpolarization techniques. The sample solutions delivered to the NMR spectrometer should be stable and homogeneous to allow for the acquisition of high-quality NMR spectra. The samples need to be delivered to the NMR spectrometer within a time frame that allows for acquisition of data before decay of the enhanced spin polarization. Mixing experiments for the measurement of molecular interactions or reactions additionally require accurate final concentrations and sample volumes.

4.1. Direct sample transfer

The most straight forward uses of a hyperpolarized sample can be grouped under the label of directly transferring a sample to the NMR spectrometer (Fig. 4a). D-DNP instruments generally flow the dissolved sample from the instrument, which can be captured in a vessel or deposited in an NMR tube that may already be installed in an NMR spectrometer. The dissolved sample contains a diluted form of the originally hyperpolarized sample. Despite dilution, the signal can be much stronger than that of a pure sample of the same compound. The dissolution process provides additional benefits in alleviating the effect of the free radical polarizing agents, by reducing the radical concentration to the micromolar level. Para-hydrogen polarization can be generated external to the magnet using the hydrogenative ALTADENA, or the non-hydrogenative SABRE methods. This task is achieved by first introducing hydrogen gas into a reaction mixture prepared in an NMR tube through bubbling or through pressurization and shaking. The NMR tube is then manually transferred into an NMR spectrometer. A third modality of para-hydrogen polarization, PASADENA, occurs when hydrogenation is performed with the reaction mixture pre-installed at high field in the NMR magnet (Fig. 4b).

Most of the hyperpolarized NMR experiments are best performed using a connection for remote control between the hyperpolarizer and the NMR spectrometer. In these experiments, time is of essence both for keeping a high polarization level and reproducibility in the face of relaxation losses. Signal loss due to spin relaxation starts as soon as the hyperpolarization has been generated, therefore, the NMR pulse program should be triggered soon after transfer of the sample. All common NMR spectrometers contain digital input and output lines, such as operating at TTL (0 – 5 V) signal levels, which are accessible on a connector within the console. The pulse programs can be written to either wait for an external trigger on an input line, or to give a signal to the hyperpolarizer. D-DNP instruments will typically provide a trigger signal that can be directly connected to the NMR console to start data acquisition after automatic sample transfer. The para-hydrogen polarizer shown in Fig. 3b receives a signal from the NMR spectrometer console in order to control the path selection valves for starting and stopping the introduction of hydrogen gas to the sample tube. In the case of an instrument built by the researcher, it is recommended to electrically isolate the NMR console from the instrument by using an optocoupler device. Electrical isolation prevents damage to the NMR console in case of a problem in a digital control circuit in the device.

Because of the requirement to acquire signals immediately after hyperpolarization, the usual procedures for tuning and shimming of the NMR probe and spectrometer should be executed before the experiment using a different sample of similar composition and size. The hyperpolarized experiment can then be performed without time lost for tuning and shimming, as well as without locking.

4.2. Injection and mixing devices

While the above procedures present a means for performing experiments with liquid hyperpolarization using a minimal apparatus, accurate control over the sample transfer is best achieved using a separate injection device [62–66]. The procedures for hyperpolarization are the same as described above. After the hyperpolarization step, the sample is

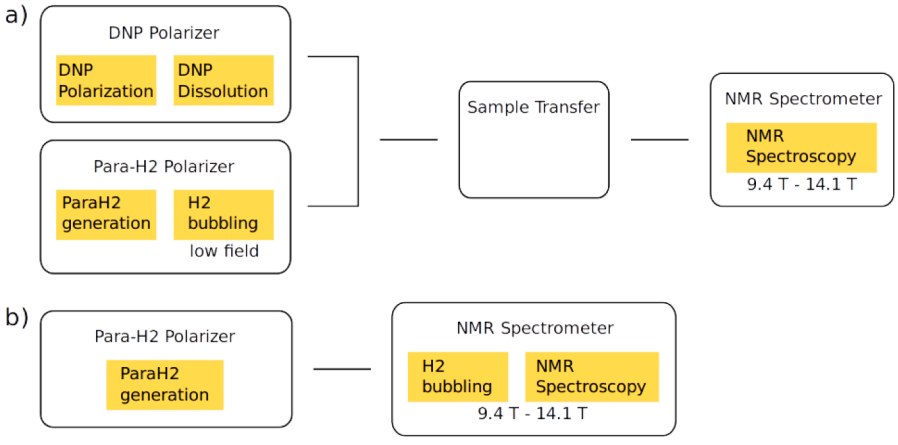

Fig. 4. Flow diagram for hyperpolarized NMR experiments. a) D-DNP or para-hydrogen polarization experiment, followed by transfer of the sample to a high-field NMR instrument. The para-hydrogen polarization in this experiment can occur through the ALTADENA (hydrogenative) or SABRE (non-hydrogenative) processes. b) Experiment employing the hydrogenative PASADENA process.

transferred to the injector device, instead of directly to the NMR instrument Fig. 5. shows flow diagrams for devices, where the sample is subsequently injected into the NMR spectrometer either using a pressurized gas or liquid. Implementations of these devices are compatible with both para-hydrogen polarization and D-DNP. These devices further facilitate admixing of another sample component during the transfer, which allows the use of hyperpolarization for the study of reactions or molecular interactions. Possible applications range from the study of biological processes and interactions to organic reactions and catalyzed organic or organometallic reactions.

Two basic schemes for rapid injection of a hyperpolarized sample into a NMR spectrometer have been implemented by our group and others. In both instances, the hyperpolarized sample is for a short time stored in a sample loop, and is subsequently pushed into the NMR spectrometer.

In a gas driven injector (Fig. 6a), the driving force for the injection is a pressurized inert gas, such as nitrogen or argon. In loading mode, the hyperpolarized sample is introduced into a sample loop (L3) and activates an optical detector once the loop is full. After the loop is filled, a two-position, 10-port valve (V3) is switched from loading into injection mode. By choosing the timing of this switching, the 0.5 – 1 mL of the hyperpolarized sample with highest signal can be selected. This part of sample is pushed into the NMR tube by applied gas pressure such as 1.8 MPa (P_f), against a back-pressure such as 1 MPa (P_b). The back-pressure serves to control the speed of injection, while keeping the overall pressure in the sample high. Thus, the formation of bubbles from gases that are dissolved in the liquid is suppressed. After an accurately timed completion of the injection sequence, typically requiring on the order of 300 – 400 ms, a two-position, three-port valve (T) is switched to step up the pressure in the NMR sample [63]. The increased pressure serves to stop the flow of residual liquid into the tube, while suppressing bubble formation during the measurement time. An additional time delay of ~100-500 ms should be included after injection and prior to triggering the NMR spectrometer to improve sample stability. This liquid motion can be quantified using pulsed gradient spin echo experiments [67].

Using this device, the hyperpolarized sample is delivered by means of gas pressure into the NMR tube, which is attached to the system through flexible tubing. The method can be applied with various NMR tube diameters, including the commonly used 5 mm and 10 mm NMR tubes. Because of elevated pressures during sample injection and measurement, the use of medium- or thick-walled NMR tubes is recommended. An advantage of this sample injection scheme is the ability to top-load the sample tubes as in a conventional NMR experiment. As the sample tubes are attached to flexible tubing for injection of the sample and for application of back-pressure, the samples are loaded manually. Appropriate personnel protection equipment, including gloves, goggles and a face shield should be worn at any time that a pressurized sample is handled.

At the same time with the sample injection, up to approximately 50 μL of a second liquid, which is pre-loaded in the NMR tube, can be mixed with the injected solution. Optimal mixing can be achieved in a 5 mm standard-walled (economy) NMR tube, to result in a final volume of the mixture of 450 – 550 μL, or in a 5 mm medium-walled NMR tube with a lower final volume of 350 – 400 μL. The significant turbulence of the injected fluid causes mixing within a time of on the order of 100 ms. The hyperpolarized sample component is thus marginally diluted, whereas the non-hyperpolarized component experiences a dilution of 10-fold or more, depending on the amount of solution pre-loaded in the NMR tube. Mixing of the non-hyperpolarized reagent with the hyperpolarized sample allows starting a reaction or causing intermolecular interactions, which can be characterized by NMR.

A liquid driven injector (Fig. 6b) pushes the hyperpolarized sample into a flow cell installed in the NMR spectrometer. The driving force is a pressurized solvent, which is delivered by the syringe pump 1. As in the gas driven case, the hyperpolarized sample is initially delivered into a sample loop (L1). Sample injection automatically occurs after switching an injection valve (V1) once the sample loop is full [64]. The flow of sample into the flow cell stops after returning the injection valve to the original position. A non-hyperpolarized sample component may be manually pre-loaded in a second loop with a typical volume of 0.4 – 1 mL (L2 attached to V2) and pushed by the syringe pump 2 during injection. This component can be mixed with the hyperpolarized sample in a Y-mixer. The duration that injector valves V1 and V2 are switched to injection position is optimized to capture the hyperpolarized sample with highest enhancement and non-hyperpolarized sample with highest concentration. The total transfer time should be as short as possible, on the order of 1000 ms, to preserve the signal enhancement from hyperpolarization. The flow-rates of the syringe pumps can be adjusted in a range of up to several hundred milliliters per minute, in order to minimize the total injection time while avoiding the injection pressure to exceed the limit of the flow cell. The use of the two sample loops and external mixer enables a broader control of mixing parameters compared to the gas driven injector. A volume ratio of 1:1 (v/v), or in principle even higher, mixing ratio between the non-hyperpolarized and the dissolved hyperpolarized sample can be achieved. This ratio is primarily limited by the achievable SNR from the diluted hyperpolarized sample. Since the liquid driven injector does not contain spaces pressurized by gases, the risk from fragments in failures due to over pressurization is reduced, but it is not eliminated. The same protective equipment should be worn as for operating the gas driven injector.

For both injection methods shown in Fig. 6, additional instrumentation in the form of an injector device is needed when compared to a direct sample transfer (Fig. 4). This instrumentation however allows for a more precise delivery of the sample, where final sample concentrations are more reproducible. Further, the time spent for the injection process is reduced to a time on the order of seconds, which reduces losses of hyperpolarization due to spin relaxation.

Injected or transferred samples present additional challenges, when compared to traditional NMR spectroscopy. The properties of the injected sample directly affect the quality of the NMR spectra that can be acquired. In both the liquid and gas driven injectors, the purpose of the loop is to select a part of the sample that contains a high concentration of

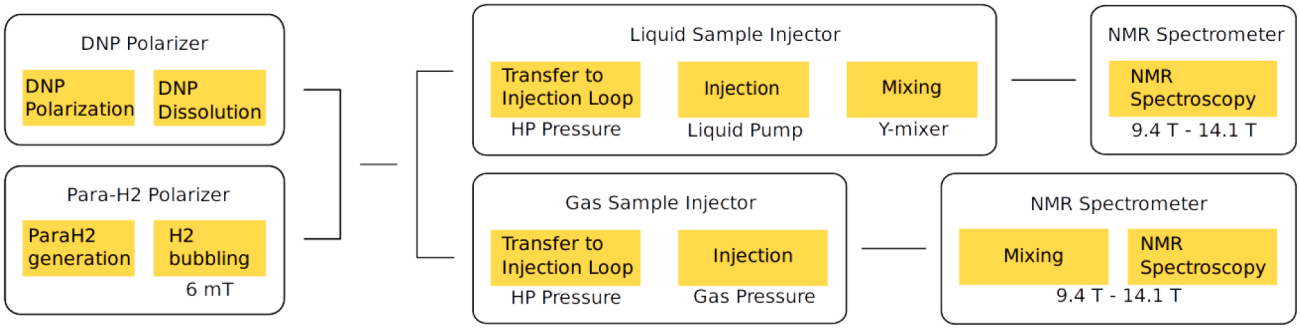

Fig. 5. Flow diagram for experimental schemes employing liquid (top) or gas driven (bottom) injection of hyperpolarized samples into an NMR spectrometer.

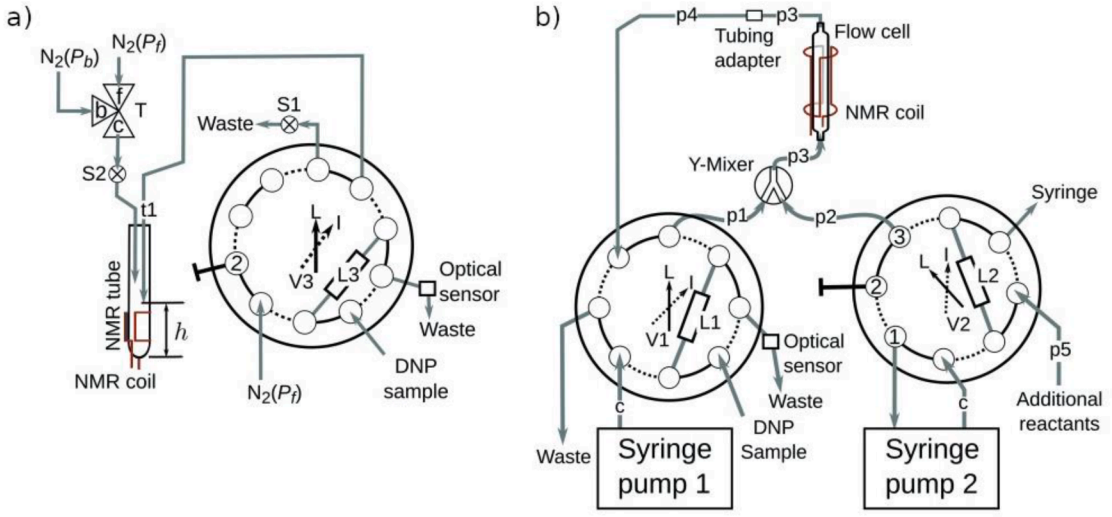

Fig. 6. Comparison of sample injection devices. a) Gas driven injector, comprising a two-position, 10-port injection valve (V3) for sample injection by applying forward pressure (P_f), sample loop (L3), two-position, 3-port valve (T) for application of back pressure (P_b). Solid lines represent loading mode (L), while dashed lines represent injection mode (I). b) Liquid driven sample injection. The hyperpolarized sample is taken into a loop (L1) as in (a), and injection is triggered. The figure is modified and reprinted from [64]. Copyright Wiley-VCH GmbH. Reproduced with permission.

the hyperpolarized compound. After injection, a sample that is free of gas bubbles is required, as the magnetic susceptibility difference between liquid and gas would result in broad lines. Both the samples from D-DNP and from para-hydrogen polarization are prone to be saturated with gasses. In the case of D-DNP, the helium chase gas can become mixed with the sample during the dissolution process. In an experiment

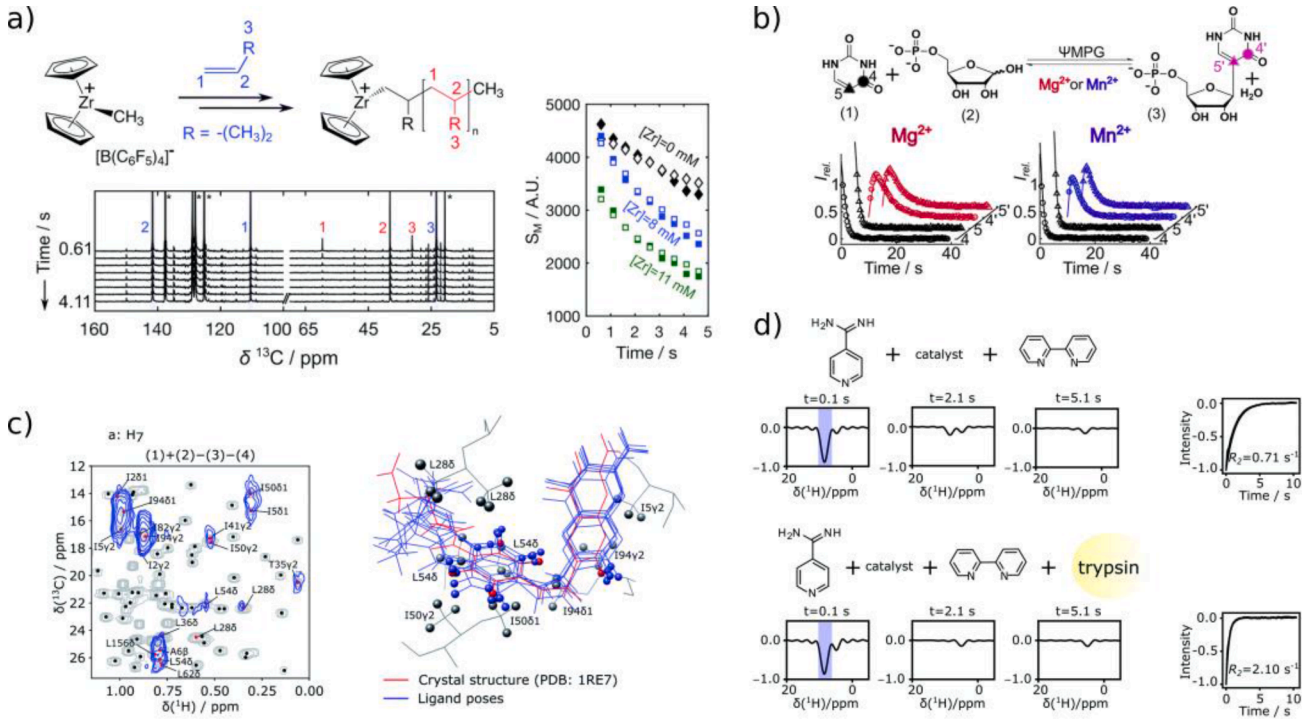

Fig. 7. Applications of rapid injection hyperpolarized NMR. a) In-situ NMR spectra of the polymerization reaction of isobutene catalyzed by the metallocene $Cp_2Zr(CH_3)$. The graph to the right shows the time dependence of NMR signals for several catalyst concentrations. Isobutene was DNP hyperpolarized on ^{13}C nuclei prior to injection and mixing with polymerization catalyst solution. b) Reaction catalyzed by the pseudouridine monophosphate glycosidase enzyme loaded with diamagnetic magnesium or paramagnetic manganese in the active site. The curves show the time dependence of the signals of ^{13}C DNP hyperpolarized reactant (1), which is isotope labeled at the positions indicated, and product (3). c) Structure of ^{1}H DNP hyperpolarized folic acid determined when binding to dihydrofolate reductase. The 2D spectrum was Hadamard reconstructed from data sets recorded after ^{1}H hyperpolarization of the folic acid ligand and NOE polarization transfer to the protein. d) Binding of the ligand 4-amidinopyridine to the trypsin protein identified by the change in the R_2 relaxation rate. The ligand was hyperpolarized by SABRE through the heterocyclic N and mixed with bipyridine to deactivate the catalyst prior to data acquisition. The experiments in (a) – (c) were performed using a gas driven sample injector, whereas (d) used a liquid driven approach. The figures are modified and reprinted from the respective sources. The panels a,c, and d are reproduced from [26,68,74] with permission from the Royal Society of Chemistry. The panel b is reprinted with permission from [69]. Copyright 2022, American Chemical Society.

with para-hydrogen, the hydrogen gas can be introduced during the polarization step at pressures that are as high as 10 bar.

In the gas driven injector described above, gas bubbles and outgassing are suppressed by the application of back-pressure during injection, which can be stepped up after injection is complete. This last step further terminates the injection in a controlled way, to achieve reproducible sample volumes. A known sample volume is important to enable shimming on a reference sample prior to the experiment. With pre-set shims, the above-described gas driven injector is capable of achieving a line width as narrow as 1.5 – 2 Hz for ^{13}C signals. Control over the injected sample volume is further required for quantitative mixing experiments. Examples of such experiments, including studies of reactions, are described below.

In the liquid driven injector, the appearance of gas bubbles is less significant. Line shape issues are further alleviated by the absence of an air-liquid interface in the flow cell. Therefore, shimming is less of a concern in this application. On the other hand, the fraction and the amount of the sample that is in the active region of the NMR coil may be smaller in a typical flow cell, compared to an NMR tube. Quantification of sample concentrations for such experiments can further be achieved by including reference compounds in the hyperpolarized samples, which can subsequently be measured by NMR or other experiments.

Apart from the different ways to achieve sample homogeneity, the liquid and gas driven injection schemes present specific advantages, and therefore specific application ranges. They are illustrated in the following Fig. 7 using selected examples from our own work. The gas driven injection in this implementation is the most rapid. Spectra can be measured after a stabilization time of on the order of 100 ms following the arrival of the sample in the NMR tube [14]. This feature can be exploited for measurements of reaction kinetics for reactions that would otherwise be too fast to be studied by NMR [28]. An example is shown in Fig. 7a, where the time course of NMR signals in a polymerization reaction of isobutene catalyzed by a metallocene catalyst is measured [68]. Signals are observed over a course of 5 s. In such experiments, a typical time resolution on the order of hundreds of milliseconds is achieved. Governed by the Nyquist sampling limit, spectra with resolvable chemical shifts could in principle be obtained in an acquisition time as short as 10 ms, which is shorter than the dead time of mixing in the experiment. Contrary to conventional stopped-flow NMR experiments, the use of hyperpolarization allows ^{13}C observation, in many cases without isotope labeling, which facilitates observing individual molecular sites due to the larger chemical shift dispersion compared to ^{1}H. In the data of Fig. 7a, a broadening in the well resolved C2 signal of isobutene was observed, which was interpreted as a result of the dynamic process of monomer insertion.

Also contrary to a conventional NMR experiment, spin relaxation that occurs at the same time as the reaction causes only a signal loss. Signals in the hyperpolarized experiment are approaching the typically unobservable signal level at thermal equilibrium, which can be approximated by zero. The effect of both reaction kinetics and these spin relaxation processes can be taken into account mathematically when analyzing data such as from Fig. 7a.

Because the driving fluid is in a different physical phase than the sample, the hyperpolarized sample is subject to no additional dilution during this injection process, or subject to a low amount of dilution when mixed with the non-hyperpolarized compound. Note that in the case of D-DNP, dilution still occurs in the dissolution process before the sample reaches the injector device. The feature of the gas driven injector not causing additional dilution is beneficial in signal limited scenarios. In signal limited cases, the signals from low-abundance nuclei may be further enhanced by isotope labeling. This option is utilized in the experiments shown in Fig. 7b, which illustrates the use of D-DNP with a gas driven sample injection scheme for the measurement of an enzyme catalyzed reaction [69]. The reaction consists of the synthesis of pseudouridine monophosphate (3) from uracil (1) and ribose-5-phosphate (2) by the action of the enzyme pseudouridine monophosphate glycosidase. The kinetic profile of the reaction is observed for enzyme that contained either magnesium or manganese in the active site. The additional paramagnetic relaxation enhancement in the presence of manganese is visible in the faster decay of the observed signals. The paramagnetic relaxation parameters from the measurements were used to calculate active site distances for the observed substrate atoms. This experiment illustrates the utility of determining both the kinetic and relaxation properties from the transient signals measured with the rapid injection method.

Fig. 7c illustrates the use of transient signals arising from nuclear Overhauser effect (NOE) transfer after rapid injection of a DNP polarized ligand into a protein solution. The observed NOEs allow the determination of the ligand structure in the binding site of the protein. The NOEs enhance specific protein signals in the binding site. The individual signals are resolved in 2D heteronuclear multi-quantum (HMQC) NMR spectra measured within a total time of approximately 5 s after completion of the gas driven sample injection. Because of the fast unbinding and rebinding of the ligand, which can be chemically in equilibrium while the hyperpolarized spin states are still far from equilibrium, continuously renewed signal is available for multiple scans for a 2D NMR spectrum. In order to utilize the observed signals from the protein for the determination of a structure, both the origin and target spins of the transferred polarization should be identified. This information would commonly be obtained from a ligand filtered 3D NOESY spectrum. Here, target selectivity is achieved by the signal gain from hyperpolarization in combination with the fast 2D NMR. In order to determine the polarization origin, Hadamard encoding of ligand signals across multiple data sets was employed. The Hadamard reconstruction requires reproducible signal intensities in the original data sets, which was facilitated by the defined injection time and volume produced by the injection device. Other experiments have been described that similarly exploit continuous polarization transfer from hyperpolarized water for signal enhancements of exchangeable amide protons in proteins [18,70,71].

In contrast to the experiment in Fig. 7c, the identification of binding without structure determination can be achieved from one-dimensional NMR spectroscopy after rapid injection of a hyperpolarized ligand into a protein solution. This goal can be achieved with DNP hyperpolarization, for example using fluoridated ligands [72]. Quantitative analysis of relaxation rates under binding competition with a reporter ligand can further be used to determine the binding affinity of a ligand [73].

The measurement of biological interactions can benefit from specific properties of the liquid driven sample injection (Fig. 6b). Specifically, physiological conditions comprise low concentrations, such that additional dilution of the hyperpolarized sample with the driving fluid (water) can easily be factored into the experiment. More importantly, the liquid driven sample injection allows for a higher mixing ratio than the gas driven experiment. For example, equal volumes of the hyperpolarized and the non-hyperpolarized sample components can be mixed. This property allows working with sample combinations where the non-hyperpolarized component has a low solubility, as can be encountered in protein solutions.

Fig. 7d illustrates an application of liquid driven sample injection for the measurement of ligand binding [74]. Here, hyperpolarization occurred through the para-hydrogen based SABRE. Although liquid driven injection is compatible with either one of the described methods, SABRE provides for a fast signal generation with low instrumentation need and low cost. The ligand in the figure is engineered to be hyperpolarizable by SABRE through the inclusion of the nitrogen atom in the aromatic ring, which provides for binding to the polarization transfer catalyst. A two-step approach was used to first hyperpolarize this substrate under conditions that are conducive for the polarization transfer catalyst in methanol-d_4 solution. Subsequently, the hyperpolarized sample was mixed with the target protein solution. Thus, the acquisition of a Carr-Purcell-Meiboom-Gill (CPMG) relaxation trace took place in a solution that is predominantly water, under biologically compatible

conditions. Secondly, relaxation effects from the polarization transfer catalyst could be neutralized using this mixing approach by including a chelating agent to trap the catalyst following the hyperpolarization step [75]. The binding of the ligand to the protein can clearly be identified by comparing the relaxation traces at the right of Fig. 7d, with the faster return to the nuclear spin state equilibrium due to the higher R_2 rate appearing when the ligand binds to the macromolecule.

The increased mixing ratio in liquid driven experiments is further of interest for the introduction of hyperpolarized compounds into cell suspensions, which can only be concentrated to a limited extent [76]. By virtue of introducing the sample through laminar flow into the flow cell, motion of the sample during the measurement time is minimized. A low amount of sample motion is important if the NMR pulse sequence makes extensive use of pulsed field gradients, such as for imaging or for spatial encoding in ultrafast pulse sequences. A rapidly abating sample motion after injection further enables the measurement of true diffusion coefficients a short time after the injection is completed [77].

The application of the sample injection device is largely independent of the chosen liquid state hyperpolarization method. Conversely, the use of the liquid driven injection device broadens the application range of para-hydrogen based polarization methods. The organometallic catalysts for para-hydrogen polarization are incompatible with sample components containing various functional groups including, for example, biological macromolecules. In the two-step procedure with liquid driven sample injection, the initial hyperpolarization step occurs under optimal conditions. The hyperpolarized sample is then mixed with the solution containing the target, such as a protein. The dilution further enables a change of the sample conditions to be compatible with the application, such as creating a primarily water-based solution for biological macromolecules even if the polarization step occurs in an organic solvent. In the same step, the polarization transfer catalyst may be inactivated to prevent interference with a reaction or other molecular process, as described above.

4.3. Additional and Alternative Experimental Procedures

The use of hyperpolarized species presents challenges that are specific to the goals of each experiment [78]. Additional variations of the sample injection scheme are possible to address specific requirements. In the case of gas driven injection, a non-hyperpolarized component can be introduced after injection through a pump [28]. This allows the application of a preparatory pulse sequence, such as using selective radio-frequency pulses for addressing specific spins, before the start of a reaction. In the case of liquid driven injection an experiment executing multiple scans on a fresh sample bolus is possible by successively advancing the injected liquid through repeated switching of the injection valve [79].

The flow injection systems are compatible with air and moisture sensitive samples. Samples can be loaded under air exclusion, in the case of using a para-hydrogen apparatus by transporting the sample container into a glove box and in the case of DNP by using capped sample holders for loading the DNP polarizer [68]. Once the sample is loaded, the injection process causes contact only with inert gases, or with solvents of desired composition.

Techniques may be used to counteract spin relaxation during sample transfer. Under certain conditions, slow-relaxing singlet states may be produced for the injection period [80] or during the NMR experiment [81]. A magnetic tunnel constructed from permanent magnets, or coils surrounding injection tubing can be used to increase the magnetic field experienced by the sample during the transfer [82]. These strategies can reduce the polarization loss, especially in the case of a long injection distance or use of nuclei prone to relaxation. In combination with the DNP technique, a further effective way of counteracting liquid state relaxation is to transfer the sample as a frozen solid, preserving the nuclear spin polarization due to a prolonged T_1 relaxation time. The DNP technique in any case produces a solid sample, which can be pneumatically pushed to the NMR spectrometer. The dissolution of the sample then occurs with predetermined volume of solvent at the site where NMR signals are acquired. This method for sample transfer can be achieved using a modified design of the insert used for DNP polarization [83].

The amount of sample recovered may be increased by the use of an immiscible liquid in the injection process. This option was demonstrated in ref [84]. for direct sample injection, but would be applicable to the liquid driven injector in Fig. 6b as well. In D-DNP experiments, the radicals that are required for the hyperpolarization step are typically unwanted during signal acquisition, as they can induce additional relaxation or potentially interact with other sample components. Due to dilution, these effects are often negligible. However, radicals may be removed by solvent extraction using the aforementioned scheme, by filtration [85,86], or non-persistent radicals may be used [87]. The development of alternative major instrumentation that brings the generation of hyperpolarization closer to the location of the acquisition of NMR spectra may reduce relaxation losses during sample transfer. A magnet containing two homogeneous centers in its magnetic field places the microwave irradiation in the same instrument as the NMR spectroscopy, thus achieving this goal [88].

Para-hydrogen polarization can be generated continuously, and thus allows for experiments requiring an on-going supply of hyperpolarized liquid. Recirculating a liquid between a hyperpolarization chamber for SABRE and a measuring flow cell permits a continuous NMR measurement [89]. A flow system that mixes para-hydrogen with a steady liquid flow of substrates over a heterogeneous hydrogenation catalyst cartridge can also constantly supply hyperpolarized substrates [90].

Another class of experiments utilizing hyperpolarized liquids aims at biomedical imaging. This modality has been applied extensively using DNP, and has been demonstrated by para-hydrogen polarization. D-DNP has been proposed for biomedical imaging applications since its inception [91], and has been employed in human MRI studies [92]. Automated injection devices have been developed for this application [93]. The use of para-hydrogen polarization was proposed for example for ^{13}C MRI [94]. As requirements for *invivo* use of a hyperpolarized agent are different from the *invitro* NMR spectroscopy experiments described, these experiments are not the focus of this review. *Invivo* experiments may be less dependent on rapid transfer of samples, as the distribution of the imaging agent after injection itself is a slower process. On the other hand, stricter requirements on sample purity, composition and delivery exist. These applications are the subject of other reviews [95–97].

5. Adaptation of NMR experiments for rapid injection

The use of liquid state hyperpolarization in combination with rapid injection techniques require adaptation of common high-resolution NMR experiments. Practical differences to conventional NMR pulse sequences include the need for minor changes, such as triggering of signal acquisition, which can readily be realized in commercial NMR spectrometers. More importantly, the non-renewable hyperpolarization of injected liquid samples limits the number of scans that can be executed. In contrast to conventional NMR, which allows signal averaging from hundreds of scans, these experiments need to be completed in a single scan or can be performed in a lower number of scans executed with small flip-angle excitation.

Small filp-angle excitation pulses only consume a small fraction of polarization and make repeated detection possible. A series of 1D-NMR data over time can be obtained by this means for reaction monitoring studies. The choice of flip angle thereby is dictated by the required number of scans and the achievable signal-to-noise ratio. The sequential application of small flip angles successively depletes the remaining hyperpolarization. A uniform distribution of signal intensities throughout a multi-scan experiment can be achieved by the application of a flip angle that increases in later scans [98].

Multi-dimensional NMR experiments can also be acquired using a

sequential scanning method. Unless the polarization is renewed by a process such as chemical exchange, the type of pulse sequence is limited to containing a single excitation pulse. Possibly, this pulse can be followed by one or more π pulses on the hyperpolarized nucleus. An application of a π/2 pulse on the other hand would destroy the hyperpolarization for subsequent scans.

An elegant method to circumvent the need for multiple sequential scans is the application of a method that spatially encodes coherences within the sample volume [99–101]. Such ultrafast NMR methods can be acquired in as little as one or two scans. These experiments have been proposed for multiple applications, including the acquisition of protein spectra. Multi-dimensional experiments acquired in a small number of scans make extended use of pulsed field gradients for coherence selection, as opposed to phase cycling.

Single-scan multi-dimensional NMR is compatible both with D-DNP [99] and para-hydrogen induced polarization [102]. The non-hydrogenative SABRE technique provides an additional opportunity for multi-dimensional NMR. Using SABRE, the substrates remain chemically unchanged after the hyperpolarization process. Therefore, introduction of fresh para-hydrogen gas is possible to renew the hyperpolarization [103,104]. SABRE requires specific magnetic field conditions for the hyperpolarization step, which may be achieved by shuttling of the sample outside of the high-field NMR magnet, or by the application of radio-frequency spin-lock techniques [105].

Spins on a target molecule, in particular a macromolecule such as a protein, can further be re-polarized by repeatedly binding hyperpolarized ligands (see Fig. 6c) or by proton exchange from hyperpolarized water. Thus, a multi-dimensional NMR spectrum can be acquired with renewed polarization in each scan. This technique requires a chemical equilibrium on a faster time scale than the spin-relaxation process. The technique can also be combined with excitation by a smaller flip-angle, such as 30° to maximize signals for a given number of scans [106].

Generally, hyperpolarization methods with rapid injection limit the number of scans, over which signals can be distributed. This limitation impedes the ability to acquire higher-dimensional spectra with three or four dimensions that are commonplace in high-resolution NMR. Pseudo-multidimensional experiments of hyperpolarized samples can be employed to provide similar information [26,107].

Hyperpolarization provides a contrast over non-hyperpolarized sample components such as solvents. Nevertheless, the high abundance of solvent spins, the chance of hyperpolarizing other compounds in the original sample mixture, as well as polarization transfer mechanisms that may occur during sample injection, may necessitate the suppression of large unwanted signals. Suppression techniques identical to those in conventional high-resolution NMR may be applied. These include saturation techniques, pulsed field gradient based methods, as well as selective excitation to avoid exciting solvent signals in the first place.

6. Low-field and non-traditional NMR applications

Hyperpolarization is independent of the magnetic field used for measurement of NMR signals. This property presents opportunities for using the described liquid hyperpolarization methods to extend applications of NMR to lower fields or non-traditional detection methods. The sensitivity of inductively detected NMR with a tuned receiver coil still depends on the magnetic field B_0, but this dependence is reduced from a factor of approximately $B_0^{7/4}$ to $B_0^{3/4}$ [2]. The reduction is because the hyperpolarization removes the field dependence of the spin polarization from the equation, while leaving the characteristics of the detection coil unchanged. Additionally to inductive detection, low-field NMR can benefit from measurement schemes involving non-inductive detection, using different types of magnetometers. These detection methods exhibit a field dependence that is more favorable to low-field measurements [108].

The application of both para-hydrogen polarization [109] and D-DNP [110] has been demonstrated in this context. Para-hydrogen polarization by the SABRE method was used for the acquisition of zero-field NMR spectra, which identifies molecules by *J*-coupling patterns [111,112]. The necessary spin polarization for zero- to ultralow-field (ZULF) NMR can also be provided by D-DNP [113]. The ZULF method produces information orthogonal to chemical shifts measured in high-field NMR. Similarly, nuclear spin optical rotation (NSOR) expands on the capabilities of NMR spectroscopy. NSOR is an optically detected NMR method, which relies on a nuclear spin induced rotation of the polarizaiton of a light beam to provide information on electronic states in the vicinity of a nuclear spin [114]. Measurements of NSOR at low magnetic field were achieved both using para-hydrogen polarization by SABRE [115], as well as using D-DNP [116].

Interest in low-field, ultralow-field and zero-field NMR is increasing for low-cost applications of imaging and spectroscopy, as well as the potential to enable the acquisition of new types of information with alternative detection methods. Liquid state hyperpolarization is poised to make inroads into the feasibility of these applications.

7. Conclusions

Liquid state nuclear spin hyperpolarization techniques have gained considerable attention in the NMR community during the past years. A host of applications has been demonstrated, ranging from the enhancement of the sensitivity for low-abundance compounds, such as metabolites, to the study of chemical reactions, macromolecular structure and dynamics, intracellular processes, molecular interactions and many other topics. This discussion does not even include the large field of biomedical imaging, which stands to benefit substantially from hyperpolarized imaging agents and tracers. Liquid state hyperpolarization represents an additional step prior to the NMR signal acquisition, thus adding to the complexity of the experiment. In many cases, the hyperpolarization is performed outside of the NMR magnet, thus requiring a rapid and accurate sample transfer discussed in this article. The addition of sample transfer mechanisms at the same time provides opportunities for the design of different types of experiments. For example, sample injection devices can be made compatible with stopped-flow type experiments, where real-time signal changes of reacting compounds can be measured.

With the utility of nuclear spin hyperpolarization demonstrated in principle for many fields, a broader adoption hinges on the accessibility of these techniques to interested researchers. Hyperpolarization by D-DNP, requires additional instrumentation, which is increasingly available at dedicated user facilities. Other techniques, in particular some para-hydrogen based methods may be implemented even in existing facilities. This method primarily requires a mechanism for transferring hyperpolarized samples, while para-hydrogen can be produced off-site. In addition to the generation of hyperpolarization, new NMR techniques are required that are capable of obtaining chemical and structural information from often short-lived signal enhancement. Many such techniques have been developed and can be implemented on modern NMR spectrometers, for example making extensive use of pulsed field gradients for encoding of spin coherences. In addition, liquid state hyperpolarization may enable a new emphasis on other experimental techniques such as low-field NMR, for which signal strength otherwise is a primary limitation. Overall, further improvements and developments that make these techniques most easily applicable, will be key to facilitate a broad range of applications.

Declaration of competing interest

Texas A&M University is applying for a patent covering aspects of the sample transfer technique for para-hydrogen polarization.

Acknowledgments

Financial support from the National Science Foundation (Grant CHE-1900406), the National Institutes of Health (Grant R01GM132655) and the Welch Foundation (Grant A-1658) is gratefully acknowledged.

References

[1] K. Wüthrich, NMR of Proteins and Nucleic Acids, Wiley, New York, 1986.
[2] D.I. Hoult, R.E. Richards, The signal-to-noise ratio of the nuclear magnetic resonance experiment, J. Magn. Reson. 1969 24 (1976) 71–85, https://doi.org/10.1016/0022-2364(76)90233-X.
[3] D.L. Olson, T.L. Peck, A.G. Webb, R.L. Magin, J.V. Sweedler, High-Resolution Microcoil 1H-NMR for Mass-Limited, Nanoliter-Volume Samples, Science 270 (1995) 1967–1970, https://doi.org/10.1126/science.270.5244.1967.
[4] J.H. Ardenkjaer-Larsen, B. Fridlund, A. Gram, G. Hansson, L. Hansson, M. H. Lerche, R. Servin, M. Thaning, K. Golman, Increase in signal-to-noise ratio of >10,000 times in liquid-state NMR, Proc. Natl. Acad. Sci. USA 100 (2003) 10158–10163, https://doi.org/10.1073/pnas.1733835100.
[5] J.H. Ardenkjær-Larsen, S. Bowen, J.R. Petersen, O. Rybalko, M.S. Vinding, M. Ullisch, N.Chr. Nielsen, Cryogen-free dissolution dynamic nuclear polarization polarizer operating at 3.35 T, 6.70 T, and 10.1 T, Magn. Reson. Med. 81 (2019) 2184–2194, https://doi.org/10.1002/mrm.27537.
[6] C.R. Bowers, D.P. Weitekamp, Parahydrogen and synthesis allow dramatically enhanced nuclear alignment, J. Am. Chem. Soc. 109 (1987) 5541–5542, https://doi.org/10.1021/ja00252a049.
[7] R.W. Adams, J.A. Aguilar, K.D. Atkinson, M.J. Cowley, P.I.P. Elliott, S.B. Duckett, G.G.R. Green, I.G. Khazal, J. López-Serrano, D.C. Williamson, Reversible interactions with para-hydrogen enhance NMR sensitivity by polarization transfer, Science 323 (2009) 1708–1711, https://doi.org/10.1126/science.1168877.
[8] T.G. Walker, W. Happer, Spin-exchange optical pumping of noble-gas nuclei, Rev. Mod. Phys. 69 (1997) 629–642, https://doi.org/10.1103/RevModPhys.69.629.
[9] R. Kaptein, K. Dijkstra, K. Nicolay, Laser photo-CIDNP as a surface probe for proteins in solution, Nature 274 (1978) 293–294, https://doi.org/10.1038/274293a0.
[10] M.L. Hirsch, N. Kalechofsky, A. Belzer, M. Rosay, J.G. Kempf, Brute-Force Hyperpolarization for NMR and MRI, J. Am. Chem. Soc. 137 (2015) 8428–8434, https://doi.org/10.1021/jacs.5b01252.
[11] S. Meier, M. Karlsson, P.R. Jensen, M.H. Lerche, J.Ø. Duus, Metabolic pathway visualization in living yeast by DNP-NMR, Mol. Biosyst. 7 (2011) 2834, https://doi.org/10.1039/c1mb05202k.
[12] T. Harris, G. Eliyahu, L. Frydman, H. Degani, Kinetics of hyperpolarized 13C1-pyruvate transport and metabolism in living human breast cancer cells, Proc. Natl. Acad. Sci. USA 106 (2009) 18131–18136, https://doi.org/10.1073/pnas.0909049106.
[13] E. Miclet, D. Abergel, A. Bornet, J. Milani, S. Jannin, G. Bodenhausen, Toward Quantitative Measurements of Enzyme Kinetics by Dissolution Dynamic Nuclear Polarization, J. Phys. Chem. Lett. 5 (2014) 3290–3295, https://doi.org/10.1021/jz501411d.
[14] S. Bowen, C. Hilty, Time-Resolved Dynamic Nuclear Polarization Enhanced NMR Spectroscopy, Angew. Chem. Int. Ed. 47 (2008) 5235–5237, https://doi.org/10.1002/anie.200801492.
[15] M. Ragavan, L.I. Iconaru, C.-G. Park, R.W. Kriwacki, C. Hilty, Real-time analysis of folding upon binding of a disordered protein by using dissolution DNP NMR spectroscopy, Angew. Chem. Int. Ed. 56 (2017) 7070–7073, https://doi.org/10.1002/anie.201700464.
[16] H.-Y. Chen, M. Ragavan, C. Hilty, Protein Folding Studied by Dissolution Dynamic Nuclear Polarization, Angew. Chem. Int. Ed. 52 (2013) 9192–9195, https://doi.org/10.1002/anie.201301851.
[17] M. Novakovic, G.L. Olsen, G. Pintér, D. Hymon, B. Fürtig, H. Schwalbe, L. Frydman, A 300-fold enhancement of imino nucleic acid resonances by hyperpolarized water provides a new window for probing RNA refolding by 1D and 2D NMR, Proc. Natl. Acad. Sci. USA 117 (2020) 2449–2455.
[18] D. Kurzbach, E. Canet, A.G. Flamm, A. Jhajharia, E.M.M. Weber, R. Konrat, G. Bodenhausen, Investigation of Intrinsically Disordered Proteins through Exchange with Hyperpolarized Water, Angew. Chem. Int. Ed. 56 (2017) 389–392, https://doi.org/10.1002/anie.201608903.
[19] A. Bornet, M. Maucourt, C. Deborde, D. Jacob, J. Milani, B. Vuichoud, X. Ji, J.-N. Dumez, A. Moing, G. Bodenhausen, S. Jannin, P. Giraudeau, Highly Repeatable Dissolution Dynamic Nuclear Polarization for Heteronuclear NMR Metabolomics, Anal. Chem. 88 (2016) 6179–6183, https://doi.org/10.1021/acs.analchem.6b01094.
[20] A. Dey, B. Charrier, E. Martineau, C. Deborde, E. Gandriau, A. Moing, D. Jacob, D. Eshchenko, M. Schnell, R. Melzi, D. Kurzbach, M. Ceillier, Q. Chappuis, S. F. Cousin, J.G. Kempf, S. Jannin, J.-N. Dumez, P. Giraudeau, Hyperpolarized NMR Metabolomics at Natural 13C Abundance, Anal. Chem 92 (2020) 14867–14871, https://doi.org/10.1021/acs.analchem.0c03510.
[21] M. Karlsson, J.H. Ardenkjær-Larsen, M.H. Lerche, Hyperpolarized 133 Cs is a sensitive probe for real-time monitoring of biophysical environments, Chem Commun 53 (2017) 6625–6628, https://doi.org/10.1039/C7CC02943H.
[22] Q. Chappuis, J. Milani, B. Vuichoud, A. Bornet, A.D. Gossert, G. Bodenhausen, S. Jannin, Hyperpolarized Water to Study Protein–Ligand Interactions, J. Phys. Chem. Lett. 6 (2015) 1674–1678, https://doi.org/10.1021/acs.jpclett.5b00403.
[23] H. Min, G. Sekar, C. Hilty, Polarization transfer from ligands hyperpolarized by dissolution dynamic nuclear polarization for screening in drug discovery, ChemMedChem 10 (2015) 1559–1563, https://doi.org/10.1002/cmdc.201500241.
[24] Y. Wang, C. Hilty, Amplification of Nuclear Overhauser Effect Signals by Hyperpolarization for Screening of Ligand Binding to Immobilized Target Proteins, Anal. Chem. 92 (2020) 13718–13723, https://doi.org/10.1021/acs.analchem.0c01071.
[25] Y. Lee, H. Zeng, A. Mazur, M. Wegstroth, T. Carlomagno, M. Reese, D. Lee, S. Becker, C. Griesinger, C. Hilty, Hyperpolarized Binding Pocket Nuclear Overhauser Effect for Determination of Competitive Ligand Binding, Angew. Chem. Int. Ed. 51 (2012) 5179–5182, https://doi.org/10.1002/anie.201201003.
[26] Y. Wang, J. Kim, C. Hilty, Determination of protein–ligand binding modes using fast multi-dimensional NMR with hyperpolarization, Chem. Sci. 11 (2020) 5935–5943, https://doi.org/10.1039/D0SC00266F.
[27] P.R. Jensen, S. Meier, J.H. Ardenkjær-Larsen, J.Ø. Duus, M. Karlsson, M. H. Lerche, Detection of low-populated reaction intermediates with hyperpolarized NMR, Chem. Commun. (2009) 5168, https://doi.org/10.1039/b910626j.
[28] C.-H. Chen, W.-C. Shih, C. Hilty, Situ Determination of Tacticity, Deactivation, and Kinetics in [rac-(C2H4(1-Indenyl)2)ZrMe][B(C6F5)4] and [Cp2ZrMe][B(C6F5)4]-Catalyzed Polymerization of 1-Hexene Using 13C Hyperpolarized NMR, J. Am. Chem. Soc 137 (2015) 6965–6971, https://doi.org/10.1021/jacs.5b04479.
[29] Y. Kim, C.-H. Chen, C. Hilty, Direct observation of Ru-alkylidene forming into ethylene in ring-closing metathesis from hyperpolarized 1H NMR, Chem. Commun. 54 (2018) 4333–4336, https://doi.org/10.1039/C7CC08135A.
[30] M. Gal, M. Mishkovsky, L. Frydman, Real-time monitoring of chemical transformations by ultrafast 2D NMR spectroscopy, J. Am. Chem. Soc. 128 (2006) 951–956, https://doi.org/10.1021/ja0564158.
[31] S.A. Colebrooke, S.B. Duckett, J.A.B. Lohman, Characterisation and kinetic behaviour of H2Rh(PPh3)2(μ-Cl)2Rh(PPh3)(alkene) and related binuclear complexes detected during hydrogenation studies involving parahydrogen induced polarisation, Chem. Commun. (2000) 685–686, https://doi.org/10.1039/B000607F.
[32] R. Mandal, P. Pham, C. Hilty, Nuclear Spin Hyperpolarization of NH2- and CH3-Substituted Pyridine and Pyrimidine Moieties by SABRE, ChemPhysChem 21 (2020) 2166–2172, https://doi.org/10.1002/cphc.202000483.
[33] H. Zeng, J. Xu, J. Gillen, M.T. McMahon, D. Artemov, J.-M. Tyburn, J.A. B. Lohman, R.E. Mewis, K.D. Atkinson, G.G.R. Green, S.B. Duckett, P.C.M. van Zijl, Optimization of SABRE for polarization of the tuberculosis drugs pyrazinamide and isoniazid, J. Magn. Reson. 237 (2013) 73–78, https://doi.org/10.1016/j.jmr.2013.09.012.
[34] H.J. Jeong, S. Min, H. Chae, S. Kim, G. Lee, S.K. Namgoong, K. Jeong, Signal amplification by reversible exchange for COVID-19 antiviral drug candidates, Sci. Rep. 10 (2020) 14290, https://doi.org/10.1038/s41598-020-71282-6.
[35] I.V. Skovpin, A. Svyatova, N. Chukanov, E.Y. Chekmenev, K.V. Kovtunov, I. V. Koptyug, 15N Hyperpolarization of Dalfampridine at Natural Abundance for Magnetic Resonance Imaging, Chem. – Eur. J 25 (2019) 12694–12697, https://doi.org/10.1002/chem.201902724.
[36] O.G. Salnikov, N.V. Chukanov, A. Svyatova, I.A. Trofimov, M.S.H. Kabir, J. G. Gelovani, K.V. Kovtunov, I.V. Koptyug, E.Y. Chekmenev, 15N NMR Hyperpolarization of Radiosensitizing Antibiotic Nimorazole by Reversible Parahydrogen Exchange in Microtesla Magnetic Fields, Angew. Chem. Int. Ed. 60 (2021) 2406–2413, https://doi.org/10.1002/anie.202011698.
[37] D.A. Barskiy, R.V. Shchepin, A.M. Coffey, T. Theis, W.S. Warren, B.M. Goodson, E.Y. Chekmenev, Over 20% 15 N Hyperpolarization in Under One Minute for Metronidazole, an Antibiotic and Hypoxia Probe, J. Am. Chem. Soc. 138 (2016) 8080–8083, https://doi.org/10.1021/jacs.6b04784.
[38] P.J. Rayner, P.M. Richardson, S.B. Duckett, The Detection and Reactivity of Silanols and Silanes Using Hyperpolarized 29Si Nuclear Magnetic Resonance, Angew. Chem. Int. Ed. 59 (2020) 2710–2714, https://doi.org/10.1002/anie.201915098.
[39] A.S. Lilly Thankamony, J.J. Wittmann, M. Kaushik, B. Corzilius, Dynamic nuclear polarization for sensitivity enhancement in modern solid-state NMR, Prog. Nucl. Magn. Reson. Spectrosc. (102–103) (2017) 120–195, https://doi.org/10.1016/j.pnmrs.2017.06.002.
[40] J.-B. Hövener, A.N. Pravdivtsev, B. Kidd, C.R. Bowers, S. Glöggler, K.V. Kovtunov, M. Plaumann, R. Katz-Brull, K. Buckenmaier, A. Jerschow, F. Reineri, T. Theis, R. V. Shchepin, S. Wagner, P. Bhattacharya, N.M. Zacharias, E.Y. Chekmenev, Parahydrogen-Based Hyperpolarization for Biomedicine, Angew. Chem. Int. Ed. 57 (2018) 11140–11162, https://doi.org/10.1002/anie.201711842.
[41] F. Jähnig, G. Kwiatkowski, M. Ernst, Conceptual and instrumental progress in dissolution DNP, J. Magn. Reson. 264 (2016) 22–29, https://doi.org/10.1016/j.jmr.2015.12.024.
[42] F. Jähnig, G. Kwiatkowski, A. Däpp, A. Hunkeler, B.H. Meier, S. Kozerke, M. Ernst, Dissolution DNP using trityl radicals at 7 T field, Phys. Chem. Chem. Phys. 19 (2017) 19196–19204, https://doi.org/10.1039/C7CP03633G.
[43] J.H. Ardenkjaer-Larsen, I. Laursen, I. Leunbach, G. Ehnholm, L.-G. Wistrand, J. S. Petersson, K. Golman, EPR and DNP Properties of Certain Novel Single Electron Contrast Agents Intended for Oximetric Imaging, J. Magn. Reson. 133 (1998) 1–12, https://doi.org/10.1006/jmre.1998.1438.
[44] A. Bornet, S. Jannin, Optimizing dissolution dynamic nuclear polarization, J. Magn. Reson. 264 (2016) 13–21, https://doi.org/10.1016/j.jmr.2015.12.007.
[45] E.V. Kryukov, M.E. Newton, K.J. Pike, D.R. Bolton, R.M. Kowalczyk, A.P. Howes, M.E. Smith, R. Dupree, DNP enhanced NMR using a high-power 94 GHz

microwave source: a study of the TEMPOL radical in toluene, Phys. Chem. Chem. Phys. 12 (2010) 5757–5765, https://doi.org/10.1039/C003189E.
[46] K.-N. Hu, G.T. Debelouchina, A.A. Smith, R.G. Griffin, Quantum mechanical theory of dynamic nuclear polarization in solid dielectrics, J. Chem. Phys. 134 (2011), 125105, https://doi.org/10.1063/1.3564920.
[47] B. Corzilius, Theory of solid effect and cross effect dynamic nuclear polarization with half-integer high-spin metal polarizing agents in rotating solids, Phys. Chem. Chem. Phys. 18 (2016) 27190–27204, https://doi.org/10.1039/C6CP04621E.
[48] A.J.P. Linde, A. Bornet, J. Milani, B. Vuichoud, R. Melzi, S. Jannin, G. Bodenhausen, Cross polarization from 1H to quadrupolar 6Li nuclei for dissolution DNP, Phys. Chem. Chem. Phys. 16 (2014) 24813–24817, https://doi.org/10.1039/C4CP03592E.
[49] T. Chakrabarty, N. Goldin, A. Feintuch, L. Houben, M. Leskes, Paramagnetic Metal-Ion Dopants as Polarization Agents for Dynamic Nuclear Polarization NMR Spectroscopy in Inorganic Solids, ChemPhysChem 19 (2018) 2139–2142, https://doi.org/10.1002/cphc.201800462.
[50] M. Ragavan, H.-Y. Chen, G. Sekar, C. Hilty, Solution NMR of Polypeptides Hyperpolarized by Dynamic Nuclear Polarization, Anal. Chem. 83 (2011) 6054–6059, https://doi.org/10.1021/ac201122k.
[51] J. Natterer, J. Bargon, Parahydrogen induced polarization, Prog. Nucl. Magn. Reson. Spectrosc. 31 (1997) 293–315, https://doi.org/10.1016/S0079-6565(97)00007-1.
[52] S.B. Duckett, C.L. Newell, R. Eisenberg, Observation of New Intermediates in Hydrogenation Catalyzed by Wilkinson's Catalyst, RhCl(PPh3)3, Using Parahydrogen-Induced Polarization, J. Am. Chem. Soc. 116 (1994) 10548–10556, https://doi.org/10.1021/ja00102a023.
[53] M.J. Cowley, R.W. Adams, K.D. Atkinson, M.C.R. Cockett, S.B. Duckett, G.G. R. Green, J.A.B. Lohman, R. Kerssebaum, D. Kilgour, R.E. Mewis, Iridium N-Heterocyclic Carbene Complexes as Efficient Catalysts for Magnetization Transfer from para-Hydrogen, J. Am. Chem. Soc. 133 (2011) 6134–6137, https://doi.org/10.1021/ja200299u.
[54] A.N. Pravdivtsev, K.L. Ivanov, A.V. Yurkovskaya, P.A. Petrov, H.-H. Limbach, R. Kaptein, H.-M. Vieth, Spin polarization transfer mechanisms of SABRE: A magnetic field dependent study, J. Magn. Reson. 261 (2015) 73–82, https://doi.org/10.1016/j.jmr.2015.10.006.
[55] C.M. Wong, M. Fekete, R. Nelson-Forde, M.R.D. Gatus, P.J. Rayner, A. C. Whitwood, S.B. Duckett, B.A. Messerle, Harnessing asymmetric N-heterocyclic carbene ligands to optimise SABRE hyperpolarisation, Catal. Sci. Technol. 8 (2018) 4925–4933, https://doi.org/10.1039/C8CY01214H.
[56] J.F.P. Colell, A.W.J. Logan, Z. Zhou, J.R. Lindale, R. Laasner, R.V. Shchepin, E. Y. Chekmenev, V. Blum, W.S. Warren, S.J. Malcolmson, T. Theis, Rational ligand choice extends the SABRE substrate scope, Chem. Commun. 56 (2020) 9336–9339, https://doi.org/10.1039/D0CC01330G.
[57] K.R. Thurber, W.-M. Yau, R. Tycko, Low-temperature dynamic nuclear polarization at 9.4T with a 30mW microwave source, J. Magn. Reson. 204 (2010) 303–313, https://doi.org/10.1016/j.jmr.2010.03.016.
[58] T. Cheng, A.P. Gaunt, I. Marco-Rius, M. Gehrung, A.P. Chen, J.J. van der Klink, A. Comment, A multisample 7 T dynamic nuclear polarization polarizer for preclinical hyperpolarized MR, NMR Biomed 33 (2020), https://doi.org/10.1002/nbm.4264 e4264.
[59] R.G. Griffin, T.F. Prisner, High field dynamic nuclear polarization—the renaissance, Phys. Chem. Chem. Phys. 12 (2010) 5737–5740, https://doi.org/10.1039/C0CP90019B.
[60] J.-B. Hövener, S. Bär, J. Leupold, K. Jenne, D. Leibfritz, J. Hennig, S.B. Duckett, D. von Elverfeldt, A continuous-flow, high-throughput, high-pressure parahydrogen converter for hyperpolarization in a clinical setting, NMR Biomed 26 (2013) 124–131, https://doi.org/10.1002/nbm.2827.
[62] S. Katsikis, I. Marin-Montesinos, M. Pons, C. Ludwig, U.L. Günther, Improved Stability and Spectral Quality in Ex Situ Dissolution DNP Using an Improved Transfer Device, Appl. Magn. Reson. 46 (2015) 723–729, https://doi.org/10.1007/s00723-015-0680-5.
[63] S. Bowen, C. Hilty, Rapid sample injection for hyperpolarized NMR spectroscopy, Phys. Chem. Chem. Phys. 12 (2010) 5766–5770, https://doi.org/10.1039/C002316G.
[64] H.-Y. Chen, C. Hilty, Implementation and Characterization of Flow Injection in Dissolution Dynamic Nuclear Polarization NMR Spectroscopy, ChemPhysChem 16 (2015) 2646–2652, https://doi.org/10.1002/cphc.201500292.
[65] M. Ceillier, O. Cala, T. El Daraï, S.F. Cousin, Q. Stern, S. Guibert, S.J. Elliott, A. Bornet, B. Vuichoud, J. Milani, C. Pages, D. Eshchenko, J.G. Kempf, C. Jose, S. A. Lambert, S. Jannin, An automated system for fast transfer and injection of hyperpolarized solutions, J. Magn. Reson. Open. (8–9) (2021), 100017, https://doi.org/10.1016/j.jmro.2021.100017.
[66] G. Olsen, E. Markhasin, O. Szekely, C. Bretschneider, L. Frydman, Optimizing water hyperpolarization and dissolution for sensitivity-enhanced 2D biomolecular NMR, J. Magn. Reson. 264 (2016) 49–58, https://doi.org/10.1016/j.jmr.2016.01.005.
[67] J. Granwehr, R. Panek, J. Leggett, W. Köckenberger, Quantifying the transfer and settling in NMR experiments with sample shuttling, J. Chem. Phys. 132 (2010), 244507, https://doi.org/10.1063/1.3446804.
[68] Y. Kim, H. Samouei, C. Hilty, Polyolefin catalysis of propene, 1-butene and isobutene monitored using hyperpolarized NMR, Chem. Sci. (2021), https://doi.org/10.1039/D0SC05408A.
[69] M. Liu, G. Zhang, N. Mahanta, Y. Lee, C. Hilty, Measurement of Kinetics and Active Site Distances in Metalloenzymes Using Paramagnetic NMR with 13C Hyperpolarization, J. Phys. Chem. Lett. 9 (2018) 2218–2221, https://doi.org/10.1021/acs.jpclett.8b00350.
[70] O. Szekely, G.L. Olsen, M. Novakovic, R. Rosenzweig, L. Frydman, Assessing Site-Specific Enhancements Imparted by Hyperpolarized Water in Folded and Unfolded Proteins by 2D HMQC NMR, J. Am. Chem. Soc. 142 (2020) 9267–9284, https://doi.org/10.1021/jacs.0c00807.
[71] J. Kim, R. Mandal, C. Hilty, Observation of Fast Two-Dimensional NMR Spectra during Protein Folding Using Polarization Transfer from Hyperpolarized Water, J. Phys. Chem. Lett. 10 (2019) 5463–5467, https://doi.org/10.1021/acs.jpclett.9b02197.
[72] Y. Lee, H. Zeng, S. Ruedisser, A.D. Gossert, C. Hilty, Nuclear Magnetic Resonance of Hyperpolarized Fluorine for Characterization of Protein–Ligand Interactions, J. Am. Chem. Soc. 134 (2012) 17448–17451, https://doi.org/10.1021/ja308437h.
[73] Y. Kim, C. Hilty, Affinity Screening Using Competitive Binding with Fluorine-19 Hyperpolarized Ligands, Angew. Chem. Int. Ed. 54 (2015) 4941–4944, https://doi.org/10.1002/anie.201411424.
[74] R. Mandal, P. Pham, C. Hilty, Characterization of protein–ligand interactions by SABRE, Chem. Sci. 12 (2021) 12950–12958, https://doi.org/10.1039/D1SC03404A.
[75] R.E. Mewis, M. Fekete, G.G.R. Green, A.C. Whitwood, S.B. Duckett, Deactivation of signal amplification by reversible exchange catalysis, progress towards in vivo application, Chem. Commun. 51 (2015) 9857–9859, https://doi.org/10.1039/C5CC01896J.
[76] M. Liu, C. Hilty, Metabolic Measurements of Nonpermeating Compounds in Live Cells Using Hyperpolarized NMR, Anal. Chem. 90 (2018) 1217–1222, https://doi.org/10.1021/acs.analchem.7b03901.
[77] G. Zhang, S. Ahola, M.H. Lerche, V.-V. Telkki, C. Hilty, Identification of Intracellular and Extracellular Metabolites in Cancer Cells Using 13C Hyperpolarized Ultrafast Laplace NMR, Anal. Chem. 90 (2018) 11131–11137, https://doi.org/10.1021/acs.analchem.8b03096.
[78] P. Berthault, C. Boutin, C. Martineau-Corcos, G. Carret, Use of dissolved hyperpolarized species in NMR: Practical considerations, Prog. Nucl. Magn. Reson. Spectrosc. (118–119) (2020) 74–90, https://doi.org/10.1016/j.pnmrs.2020.03.002.
[79] H.-Y. Chen, C. Hilty, Hyperpolarized Hadamard Spectroscopy Using Flow NMR, Anal. Chem 85 (2013) 7385–7390, https://doi.org/10.1021/ac401293n.
[80] W.S. Warren, E. Jenista, R.T. Branca, X. Chen, Increasing Hyperpolarized Spin Lifetimes Through True Singlet Eigenstates, Science 323 (2009) 1711–1714, https://doi.org/10.1126/science.1167693.
[81] G. Pileio, S. Bowen, C. Laustsen, M.C.D. Tayler, J.T. Hill-Cousins, L.J. Brown, R.C. D. Brown, J.H. Ardenkjaer-Larsen, M.H. Levitt, Recycling and Imaging of Nuclear Singlet Hyperpolarization, J. Am. Chem. Soc. 135 (2013) 5084–5088, https://doi.org/10.1021/ja312333v.
[82] J. Milani, B. Vuichoud, A. Bornet, P. Miéville, R. Mottier, S. Jannin, G. Bodenhausen, A magnetic tunnel to shelter hyperpolarized fluids, Rev. Sci. Instrum. 86 (2015), 024101, https://doi.org/10.1063/1.4908196.
[83] K. Kouřil, H. Kouřilová, S. Bartram, M.H. Levitt, B. Meier, Scalable dissolution-dynamic nuclear polarization with rapid transfer of a polarized solid, Nat. Commun. 10 (2019) 1733, https://doi.org/10.1038/s41467-019-09726-5.
[84] T. Harris, C. Bretschneider, L. Frydman, Dissolution DNP NMR with solvent mixtures: Substrate concentration and radical extraction, J. Magn. Reson. 211 (2011) 96–100, https://doi.org/10.1016/j.jmr.2011.04.001.
[85] B. Vuichoud, A. Bornet, F. deNanteuil, J. Milani, E. Canet, X. Ji, P. Miéville, E. Weber, D. Kurzbach, A. Flamm, R. Konrat, A.D. Gossert, S. Jannin, G. Bodenhausen, Filterable Agents for Hyperpolarization of Water, Metabolites, and Proteins, Chem. - Eur. J 22 (2016) 14696–14700, https://doi.org/10.1002/chem.201602506.
[86] D. Gajan, A. Bornet, B. Vuichoud, J. Milani, R. Melzi, H.A. van Kalkeren, L. Veyre, C. Thieuleux, M.P. Conley, W.R. Gruning, M. Schwarzwalder, A. Lesage, C. Coperet, G. Bodenhausen, L. Emsley, S. Jannin, Hybrid polarizing solids for pure hyperpolarized liquids through dissolution dynamic nuclear polarization, Proc. Natl. Acad. Sci. USA 111 (2014) 14693–14697, https://doi.org/10.1073/pnas.1407730111.
[87] A. Capozzi, S. Patel, C.P. Gunnarsson, I. Marco-Rius, A. Comment, M. Karlsson, M. H. Lerche, O. Ouari, J.H. Ardenkjær-Larsen, Efficient Hyperpolarization of U-13C-Glucose Using Narrow-Line UV-Generated Labile Free Radicals, Angew. Chem. Int. Ed. 58 (2019) 1334–1339, https://doi.org/10.1002/anie.201810522.
[88] J. Leggett, R. Hunter, J. Granwehr, R. Panek, A.J. Perez-Linde, A.J. Horsewill, J. McMaster, G. Smith, W. Köckenberger, A dedicated spectrometer for dissolution DNP NMR spectroscopy, Phys. Chem. Chem. Phys. 12 (2010) 5883, https://doi.org/10.1039/c002566f.
[89] R.E. Mewis, K.D. Atkinson, M.J. Cowley, S.B. Duckett, G.G.R. Green, R.A. Green, L.A.R. Highton, D. Kilgour, L.S. Lloyd, J.A.B. Lohman, D.C. Williamson, Probing signal amplification by reversible exchange using an NMR flow system, Magn. Reson. Chem. 52 (2014) 358–369, https://doi.org/10.1002/mrc.4073.
[90] W.G. Hale, T.Y. Zhao, D. Choi, M.-J. Ferrer, B. Song, H. Zhao, H.E. Hagelin-Weaver, C.R. Bowers, Toward Continuous-Flow Hyperpolarisation of Metabolites via Heterogenous Catalysis, Side-Arm-Hydrogenation, and Membrane Dissolution of Parahydrogen, ChemPhysChem 22 (2021) 822–827, https://doi.org/10.1002/cphc.202100119.
[91] K. Golman, J.S. Petersson, P. Magnusson, E. Johansson, P. Åkeson, C.-M. Chai, G. Hansson, S. Månsson, Cardiac metabolism measured noninvasively by hyperpolarized 13C MRI, Magn. Reson. Med. 59 (2008) 1005–1013, https://doi.org/10.1002/mrm.21460.
[92] S.J. Nelson, J. Kurhanewicz, D.B. Vigneron, P.E.Z. Larson, A.L. Harzstark, M. Ferrone, M. van Criekinge, J.W. Chang, R. Bok, I. Park, G. Reed, L. Carvajal, E. J. Small, P. Munster, V.K. Weinberg, J.H. Ardenkjaer-Larsen, A.P. Chen, R.

E. Hurd, L.-I. Odegardstuen, F.J. Robb, J. Tropp, J.A. Murray, Metabolic imaging of patients with prostate cancer using hyperpolarized [1-13C]pyruvate, Sci. Transl. Med. 5 (2013), https://doi.org/10.1126/scitranslmed.3006070, 198ra108.
[93] A. Comment, Dissolution DNP for in vivo preclinical studies, J. Magn. Reson. 264 (2016) 39–48, https://doi.org/10.1016/j.jmr.2015.12.027.
[94] K. Golman, O. Axelsson, H. Jóhannesson, S. Månsson, C. Olofsson, J.S. Petersson, Parahydrogen-induced polarization in imaging: Subsecond 13C angiography, Magn. Reson. Med 46 (2001) 1–5, https://doi.org/10.1002/mrm.1152.
[95] A.B. Schmidt, C.R. Bowers, K. Buckenmaier, E.Y. Chekmenev, H. de Maissin, J. Eills, F. Ellermann, S. Glöggler, J.W. Gordon, S. Knecht, I.V. Koptyug, J. Kuhn, A.N. Pravdivtsev, F. Reineri, T. Theis, K. Them, J.-B. Hövener, Instrumentation for Hydrogenative Parahydrogen-Based Hyperpolarization Techniques, Anal. Chem. 94 (2022) 479–502, https://doi.org/10.1021/acs.analchem.1c04863.
[96] K.R. Keshari, D.M. Wilson, Chemistry and biochemistry of 13C hyperpolarized magnetic resonance using dynamic nuclear polarization, Chem. Soc. Rev. 43 (2014) 1627–1659, https://doi.org/10.1039/C3CS60124B.
[97] R.E. Hurd, Y.-F. Yen, A. Chen, J.H. Ardenkjaer-Larsen, Hyperpolarized 13C metabolic imaging using dissolution dynamic nuclear polarization, J. Magn. Reson. Imaging. 36 (2012) 1314–1328, https://doi.org/10.1002/jmri.23753.
[98] H. Zeng, S. Bowen, C. Hilty, Sequentially acquired two-dimensional NMR spectra from hyperpolarized sample, J. Magn. Reson. 199 (2009) 159–165, https://doi.org/10.1016/j.jmr.2009.04.011.
[99] L. Frydman, D. Blazina, Ultrafast two-dimensional nuclear magnetic resonance spectroscopy of hyperpolarized solutions, Nat. Phys. 3 (2007) 415–419, https://doi.org/10.1038/nphys597.
[100] K. Singh, C. Jacquemmoz, P. Giraudeau, L. Frydman, J.-N. Dumez, Ultrafast 2D 1H–1H NMR spectroscopy of DNP-hyperpolarised substrates for the analysis of mixtures, Chem. Commun. 57 (2021) 8035–8038, https://doi.org/10.1039/D1CC03079E.
[101] P. Giraudeau, Y. Shrot, L. Frydman, Multiple Ultrafast, Broadband 2D NMR Spectra of Hyperpolarized Natural Products, J. Am. Chem. Soc. 131 (2009) 13902–13903, https://doi.org/10.1021/ja905096f.
[102] V. Daniele, F.-X. Legrand, P. Berthault, J.-N. Dumez, G. Huber, Single-Scan Multidimensional NMR Analysis of Mixtures at Sub-Millimolar Concentrations by using SABRE Hyperpolarization, Chemphyschem Eur, J. Chem. Phys. Phys. Chem. 16 (2015) 3413–3417, https://doi.org/10.1002/cphc.201500535.
[103] P. TomHon, E. Akeroyd, S. Lehmkuhl, E.Y. Chekmenev, T. Theis, Automated Pneumatic Shuttle for Magnetic Field Cycling and Parahydrogen Hyperpolarized Multidimensional NMR, J. Magn. Reson. 312 (2020), 106700, https://doi.org/10.1016/j.jmr.2020.106700.
[104] L.S. Lloyd, R.W. Adams, M. Bernstein, S. Coombes, S.B. Duckett, G.G.R. Green, Richard.J. Lewis, R.E. Mewis, C.J. Sleigh, Utilization of SABRE-Derived Hyperpolarization To Detect Low-Concentration Analytes via 1D and 2D NMR Methods, J. Am. Chem. Soc. 134 (2012) 12904–12907, https://doi.org/10.1021/ja3051052.
[105] A.N. Pravdivtsev, A.V. Yurkovskaya, H.-M. Vieth, K.L. Ivanov, RF-SABRE: A Way to Continuous Spin Hyperpolarization at High Magnetic Fields, J. Phys. Chem. B. 119 (2015) 13619–13629, https://doi.org/10.1021/acs.jpcb.5b03032.
[106] J. Kim, M. Liu, C. Hilty, Modeling of Polarization Transfer Kinetics in Protein Hydration Using Hyperpolarized Water, J. Phys. Chem. B. 121 (2017) 6492–6498, https://doi.org/10.1021/acs.jpcb.7b03052.
[107] S. Bowen, H. Zeng, C. Hilty, Chemical Shift Correlations from Hyperpolarized NMR by Off-Resonance Decoupling, Anal. Chem. 80 (2008) 5794–5798, https://doi.org/10.1021/ac8004567.
[108] D. Budker, M. Romalis, Optical magnetometry, Nat. Phys. 3 (2007) 227–234, https://doi.org/10.1038/nphys566.
[109] J. Colell, P. Türschmann, S. Glöggler, P. Schleker, T. Theis, M. Ledbetter, D. Budker, A. Pines, B. Blümich, S. Appelt, Fundamental aspects of parahydrogen enhanced low-field nuclear magnetic resonance, Phys. Rev. Lett. 110 (2013), 137602, https://doi.org/10.1103/PhysRevLett.110.137602.
[110] Y. Zhu, C.-H. Chen, Z. Wilson, I. Savukov, C. Hilty, Milli-tesla NMR and spectrophotometry of liquids hyperpolarized by dissolution dynamic nuclear polarization, J. Magn. Reson. 270 (2016) 71–76, https://doi.org/10.1016/j.jmr.2016.06.014.
[111] T. Theis, P. Ganssle, G. Kervern, S. Knappe, J. Kitching, M.P. Ledbetter, D. Budker, A. Pines, Parahydrogen-enhanced zero-field nuclear magnetic resonance, Nat. Phys. 7 (2011) 571–575, https://doi.org/10.1038/nphys1986.
[112] D.B. Burueva, J. Eills, J.W. Blanchard, A. Garcon, R. Picazo-Frutos, K. V. Kovtunov, I.V. Koptyug, D. Budker, Chemical Reaction Monitoring using Zero-Field Nuclear Magnetic Resonance Enables Study of Heterogeneous Samples in Metal Containers, Angew. Chem. Int. Ed. 59 (2020) 17026–17032, https://doi.org/10.1002/anie.202006266.
[113] D.A. Barskiy, M.C.D. Tayler, I. Marco-Rius, J. Kurhanewicz, D.B. Vigneron, S. Cikrikci, A. Aydogdu, M. Reh, A.N. Pravdivtsev, J.-B. Hövener, J.W. Blanchard, T. Wu, D. Budker, A. Pines, Zero-field nuclear magnetic resonance of chemically exchanging systems, Nat. Commun. 10 (2019) 3002, https://doi.org/10.1038/s41467-019-10787-9.
[114] I.M. Savukov, S.-K. Lee, M.V. Romalis, Optical detection of liquid-state NMR, Nature 442 (2006) 1021–1024, https://doi.org/10.1038/nature05088.
[115] P. Štěpánek, A.M. Kantola, Low-Concentration Measurements of Nuclear Spin-Induced Optical Rotation Using SABRE Hyperpolarization, J. Phys. Chem. Lett. 10 (2019) 5458–5462, https://doi.org/10.1021/acs.jpclett.9b02194.
[116] Y. Zhu, C. Hilty, I. Savukov, Dynamic Nuclear Polarization Enhanced Nuclear Spin Optical Rotation, Angew. Chem. Int. Ed. 60 (2021) 8823–8826, https://doi.org/10.1002/anie.202016412.
[117] J.M. Franck, A. Pavlova, J.A. Scott, S. Han, Quantitative cw Overhauser effect dynamic nuclear polarization for the analysis of local water dynamics, Prog. Nucl. Magn. Reson. Spectrosc. 74 (2013) 33–56, https://doi.org/10.1016/j.pnmrs.2013.06.001.